ribosomal RNA using $2^{-\Delta\Delta Ct}$ method (Applied Biosystems,, Foster City, CA, User Bulletin No. 2).

Immunoblot analysis

Liver tissue extracts were prepared by using M-PER® Mammalian Protein Extraction Reagent (Thermo Fisher Scientific, Rockford, IL) plus Halt™ Protease Inhibitor Cocktail (Thermo Fisher Scientific, Rockford, IL). Immunoblot analysis was performed with specific antibodies against uMtCK (dilution, 1:1,000; Abcam, Cambridge, United Kingdom) and beta-actin (dilution, 1:2,000; Sigma-Aldrich, St. Louis, MO) as described-previously.[9] Immunoreactive proteins were visualized using a chemiluminescence kit (GE Healthcare, Buckinghamshire, United Kingdom), and recorded using a LAS-4000 image analyzer (Fuji Film, Tokyo, Japan). The intensities of immunodetected bands were quantified with NIH Image J software.

Immunohistochemical analysis

Excised liver specimens were fixed immediately in 10% formalin and embedded in paraffin. Serial 4-μm-thick liver tissue sections were deparaffinized, and incubated in citrate buffer at 95°C for 40 min for antigen retrieval, and then incubated overnight at 4°C with anti-uMtCK antibody (Proteintech, Chicago, IL). Biotinylated secondary antibodies (Pharmingen, San Diego, CA) were added and incubated for 20 min at room temperature. Streptavidin–horseradish peroxidase (Pharmingen, San Diego, CA) was added and after 30 min the sections were developed with 3,3′-diaminobenzidine substrate and counterstained hematoxylin.

Patient follow-up and diagnosis of HCC

Patients were followed up at the outpatient clinic with blood tests including tumor markers every 1–3 months, and ultrasonography every 4–6 months. Contrast-enhanced CT was performed when serum tumor markers showed an abnormal rise and/or tumor(s) was detected as possible HCC on ultrasonography. The diagnosis of HCC was based on the typical findings on CT, that is, hyperattenuation in the arterial phase and hypoattenuation in the equilibrium phase.[19,20]

The end points consisted of the interval between the first measurement of serum MtCK activity and the detection of HCC development, death without HCC development or the last examination until May 30, 2013, whichever came first. Death without HCC development was treated as censored data.

Statistical analysis

Categorical data were compared by χ^2-test or Fisher's exact test. Distributions of continuous variables were analyzed with Student's *t*-test for two groups. All tests of significance were two-tailed, and $p < 0.05$ was considered statistically significant. The potential associations between the MtCK and the following factors were assessed using Spearman's rank correlation coefficient: age, serum albumin, AST, ALT, GGT, total bilirubin, AFP, DCP, platelet count, prothrombin time and liver stiffness measured by Fibroscan. Cumulative incidence of hepatocarcinogenesis was calculated by the Kaplan–Meier method, and differences among groups were assessed using the log-rank test. The following factors were assessed as candidate risk factors for hepatocarcinogenesis by time-fixed Cox proportional hazard regression: age, sex, hepatitis virus, serum albumin, AST, ALT, GGT, total bilirubin, AFP, DCP, platelet count, prothrombin time, liver stiffness and MtCK. We used univariate and multivariate time-fixed Cox proportional hazard models and stepwise variable selection based on Akaike Information Criteria. Data processing and analysis were performed using SPSS software version 17.0 or 19.0 (SPSS, Chicago, IL).

Table 1. Characteristics of the enrolled chronic hepatitis C patients

Parameter	*N* = 171
Age (year)[1]	68 (60–75.5)
Female[2]	75 (43.9)
MtCK (U/L)[1]	4.50 (3.20–7.19)
Albumin (g/dL)[1]	4.0 (3.7–4.3)
AST (U/L)[1]	40 (29–63)
ALT (U/L)[1]	35 (23–55.5)
GGT (U/L)[1]	28 (20–49.5)
Total bilirubin (mg/dL)[1]	0.8 (0.6–1.2)
AFP (ng/dL)[1]	5.0 (3.0–10.1)
DCP (mAU/mL)[1]	16 (12–22.5)
Platelet ($\times 10^4/\mu L$)[1]	12.1 (8.8–17.5)
Prothrombin time (sec)[1]	11.7 (11.2–12.5)
LSV measured by Fibroscan (kPa)[1]	10.5 (5.7–17.0)

[1]Data were expressed as mean (1st–3rd. quartile).
[2]Data were expressed as number (%).

Results

Increased serum MtCK activity in patients with chronic hepatitis C

Clinical and laboratory variables of the enrolled patients are listed in Table 1. The mean level of serum albumin and total bilirubin and the mean platelet count in the enrolled patients were 4.0 g/dL, 0.8 mg/dL and 12.1 × $10^4/\mu L$, suggesting that the patients would have developed various stages of liver fibrosis, not exclusively liver cirrhosis. In agreement with this fact, the mean liver stiffness value in the enrolled patients was 10.5 kPa, suggesting the fibrosis stage of F3.[17] In these patients, serum MtCK activity was higher than the previously reported values in healthy subjects ($p < 0.001$): the mean serum MtCK activity was 4.5 U/L in patients with chronic hepatitis C, whereas 3.4 U/L in healthy subjects as described previously.[8]

Relationships between serum MtCK activity and various parameters

Relationships between serum MtCK activity and various clinical parameters are summarized in Table 2. Serum MtCK activity was significantly correlated with serum albumin levels, platelet counts and liver stiffness values ($p < 0.001$, 0.026

Table 2. Relation between serum MtCK activity and various parameters

Parameter	Spearman's ρ	*p*-Value
Age (year)	0.1829	0.016
Albumin (g/dL)	−0.4041	<0.001
AST (U/L)	0.2419	0.0014
ALT (U/L)	0.1556	0.042
GGT (U/L)	0.0427	0.58
Total bilirubin (mg/dL)	−0.0044	0.96
AFP (ng/dL)	0.2207	0.0037
DCP (mAU/mL)	0.0667	0.39
Platelet ($\times 10^4/\mu L$)	−0.1703	0.026
Prothrombin time (sec)	0.1482	0.086
LSV measured by Fibroscan (kPa)	0.2843	<0.001

and <0.001), suggesting that the increase in serum MtCK activity may be associated with the stage of liver fibrosis. On the other hand, the significant correlations between serum MtCK activity and serum levels of AST ($p = 0.0014$) and ALT ($p = 0.042$) were observed, which may suggest that serum MtCK activity is increased in association with hepatocellular damage. Furthermore, serum MtCK activity was significantly correlated with serum AFP levels ($p = 0.0037$).

Increased uMtCK mRNA and protein expressions and immunoreactivity for uMtCK in fibrotic livers in mice

As described earlier, among two tissue-specific isozymes of MtCK, that is, uMtCK and sMtCK, we have found that the increase in serum MtCK activity in HCC patients was mostly owing to that in serum uMtCK activity but not in serum sMtCK activity.[8] As the current evidence suggests that serum MtCK activity may be increased in association with the stage of liver fibrosis, we wondered whether uMtCK expression might be enhanced in fibrotic livers. To test this hypothesis, we first measured uMtCK mRNA levels in the livers of mice treated with bile duct ligation for 4 weeks. As shown in Figure 1*a*, uMtCK mRNA levels in the livers were significantly enhanced in bile duct-ligated mice at 4 weeks after the operation compared to sham-operated mice ($p = 0.02$; Fig. 1*a*). An increased immunoreactivity for uMtCK was detected in bile duct-ligated mouse livers, predominantly in hepatocytes at the periductular area, as compared to sham-operated livers, where immunoreactivity was very low or absent (Fig. 1*b*). This increased immunoreactivity was confirmed to be owing to uMtCK protein expression by immunoblot analysis (Fig. 1*c*). These results suggest that uMtCK expression may be increased in fibrotic livers predominantly in hepatocytes, possibly leading to enhanced serum MtCK activity.

Increased serum MtCK activity as an independent risk for hepatocarcinogenesis

The enrolled patients were then followed up to detect HCC occurrence. During the mean follow-up period of 2.7 years (1st–3rd quartile: 2.4–3.1 years), HCC developed in 21 patients. To carefully exclude MtCK production by HCC, HCC was ruled out at the enrollment by ultrasonography, dynamic CT and/or magnetic resonance imaging. The cumulative incidence rates of HCC at 1, 2 and 3 years estimated by the Kaplan–Meier method were 3.5, 8.8 and 12.3%, respectively, as shown in Figure 2*a*. In these patients who developed HCC, serum MtCK activity was significantly higher than that in patients who did not develop HCC ($p < 0.001$) as shown in Figure 2*b*; serum MtCK activity was 10.6 U/L (interquartile range, 4.4–20.7) in patients who developed HCC and 4.3 U/L (interquartile range, 3.1–6.6) in patients who did not develop HCC. Then, significant risk factors for HCC occurrence by univariate Cox regression analysis were as follows (Table 3): older age ($p = 0.018$), lower albumin ($p < 0.001$), higher AST ($p = 0.017$), higher AFP ($p < 0.001$), lower platelet count ($p = 0.0025$), longer prothrombin time ($p = 0.0013$), elevated liver stiffness value ($p < 0.001$) and higher serum MtCK activity ($p < 0.001$). Multivariate analysis using stepwise variable selection based on Akaike Information Criteria identified higher serum MtCK activity (HR: 1.09/year, $p < 0.001$), higher AFP (HR: 1.01/year, $p = 0.002$) and longer prothrombin time (HR: 1.48/year, $p = 0.002$) as the significant risk factors.

As our multivariate analysis identified serum MtCK activity as an independent factor associated with a risk for HCC development, we determined a cutoff value of serum MtCK activity for the prediction of HCC development by receiver operating characteristics (ROC) analysis. From this analysis, serum MtCK activity of 9.0 U/L was identified as a cutoff value (Fig. 3*a*), and with this cutoff value, area under receiver operating characteristics curve for serum MtCK activity was 0.754 (95% confidence interval [CI]: 0.613–0.894), with a sensitivity of 61.9%, a specificity of 92.8%, a positive predictive value of 56.5% and a negative predictive value of 94.2%. As this negative predictive value was high, the patients with serum MtCK activity of ≤9.0 U/L are suggested to be at a lower risk for HCC development. In fact, as shown in Figure 3*b*, patients with serum MtCK activity of >9.0 U/L were at a significantly higher risk for HCC development compared to those with serum MtCK activity of ≤9.0 U/L ($p < 0.001$). As serum MtCK activity seemed to be correlated with liver fibrosis as observed above, a relationship between serum MtCK activity and HCC development was analyzed in stratified patients by liver stiffness values. As shown in Figures 3*c* and 3*d*, in both patient groups with liver stiffness values of >15 and ≤15 kPa, serum MtCK activity of >9.0 U/L was a significantly higher risk for HCC development compared to those with serum MtCK activity of ≤9.0 U/L ($p < 0.001$). Notably, the cumulative incidence of HCC at 1,100 days of follow-up period in patients with serum MtCK activity of >9.0 U/L was comparable, approximately 0.5, irrespective of their liver stiffness values, that is ≤15 or >15 kPa. Collectively, the higher serum MtCK activity may be an independent risk for HCC development in chronic hepatitis C patients.

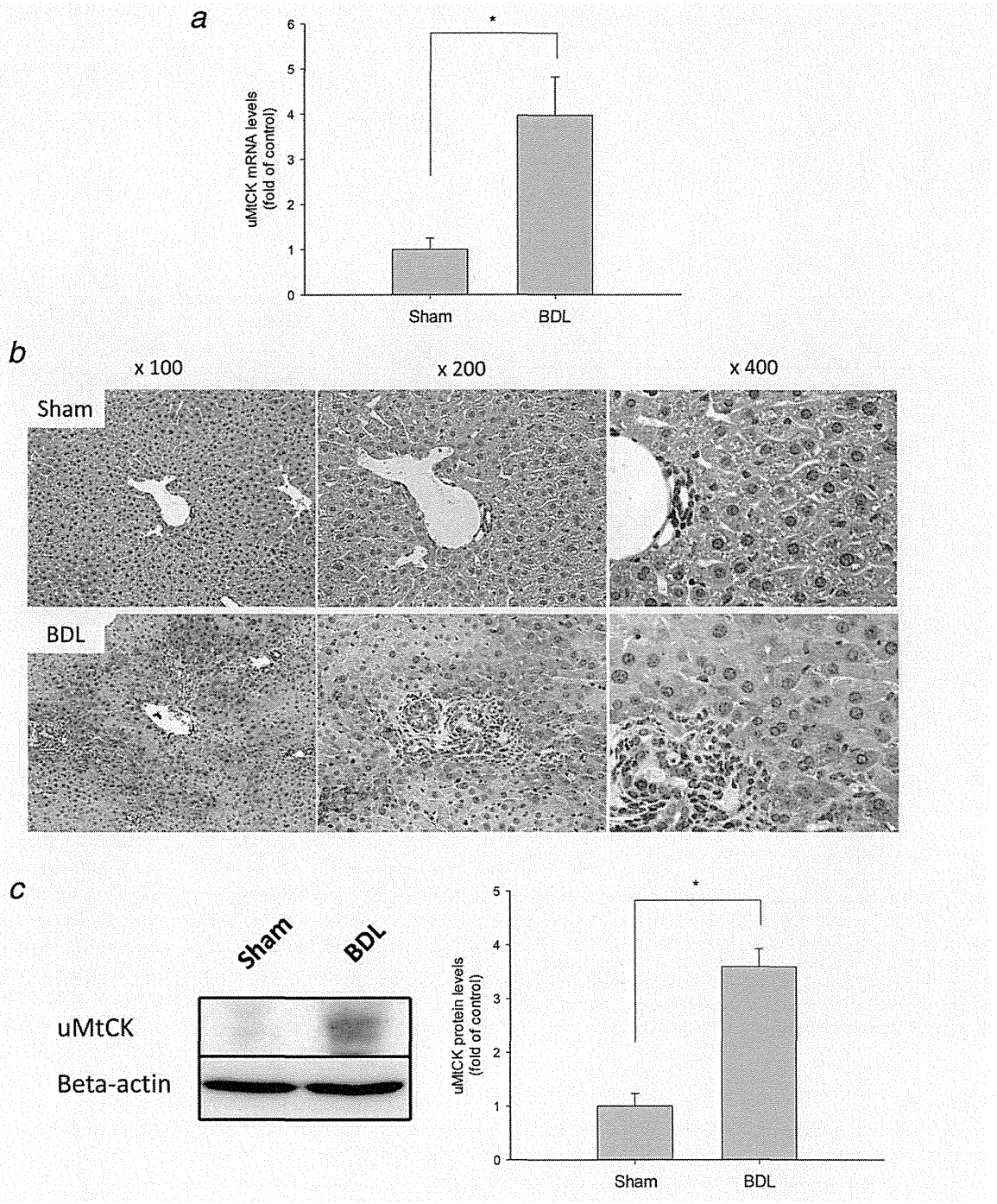

Figure 1. uMtCK mRNA and protein expressions in fibrotic livers induced by bile duct ligation in mice. (*a*) uMtCK mRNA expressions were evaluated by quantitative real-time PCR in the livers of bile duct-ligated and sham-operated mice at 4 weeks after the operation. Results represent a fold of control mice (means ± SEM, $n = 4$). uMtCK mRNA expressions were significantly enhanced in fibrotic livers induced by bile duct ligation in mice ($p = 0.02$) compared to control livers; an asterisk indicates a significant difference. (*b*) uMtCK protein expressions were evaluated immunohistochemically in fibrotic livers induced by bile duct ligation in mice in comparison with control livers. Increased immunoreactivity for uMtCK was observed predominantly in hepatocytes in fibrotic livers compared to control livers. (*c*) uMtCK protein expressions, evaluated by immmunoblot analysis, were significantly enhanced in fibrotic livers induced by bile duct ligation in mice ($p = 0.03$) compared to control livers; an asterisk indicates a significant difference.

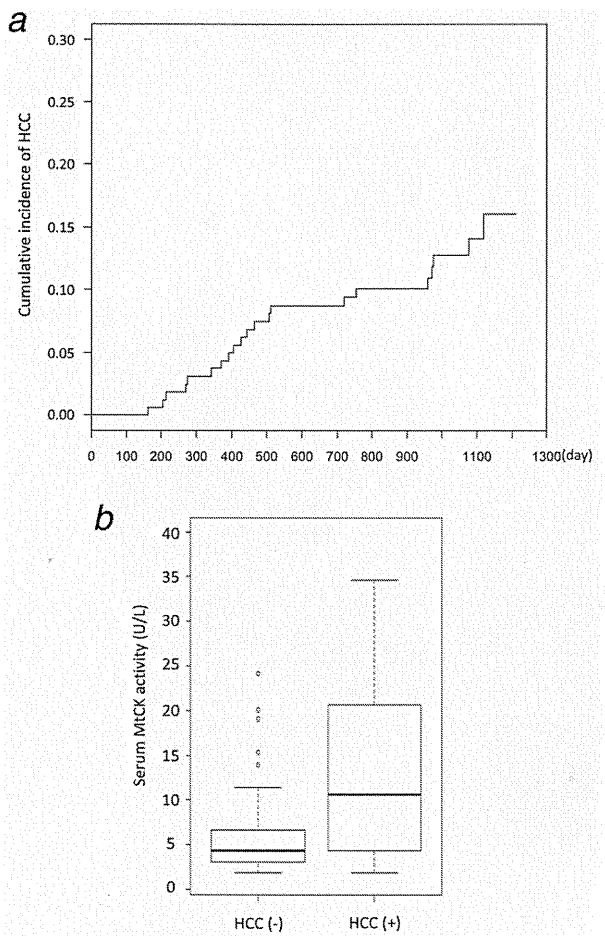

Figure 2. Serum MtCK activity and HCC development in chronic hepatitis C patients. (*a*) Cumulative incidence of HCC in chronic hepatitis C patients. During the mean follow-up period of 2.7 years, HCC developed in 21 patients. The cumulative incidence rates of HCC at 1, 2 and 3 years estimated by the Kaplan–Meier method were 3.5, 8.8 and 12.3%, respectively. (*b*) Serum MtCK activity in chronic hepatitis C patients with or without HCC development. The mean serum MtCK activity in patients with HCC development was 10.6 U/L and significantly higher than that in patients without HCC development, 4.3 U/L ($p < 0.001$).

Table 3. Risk factors for HCC evaluated by univariate and multivariate analyses

	Univariate		Multivariate	
Parameter	HR (95% CI)	*p*-Value	HR (95% CI)	*p*-Value
Age (year)	1.06 (1.01–1.12)	0.018	1.04 (0.98–1.09)	0.28
Female	0.74 (0.31–1.78)	0.50		
MtCK (U/L)	1.08 (1.05–1.11)	<0.001	1.09 (1.04–1.13)	<0.001
Albumin (g/dL)	0.15 (0.07–0.36)	<0.001		
AST (U/L)	1.01 (1.00–1.02)	0.017		
ALT (U/L)	1.002 (0.998–1.010)	0.66		
GGT (U/L)	1.001 (0.997–1.006)	0.54		
Total bilirubin (mg/dL)	2.36 (0.99–5.61)	0.053		
AFP (ng/dL)	1.02 (0.98–1.02)	<0.001	1.01 (1.004–1.02)	0.002
DCP (mAU/mL)	1.02 (0.98–1.04)	0.020		
Platelet ($\times 10^4/\mu L$)	0.87 (0.80–0.95)	0.0025		
Prothrombin time (sec)	1.53 (1.18–1.98)	0.0013	1.48 (1.28–1.91)	0.002
LSV (kPa)	1.06 (1.04–1.08)	<0.001		

Discussion

In our study, we aimed to explore the clinical significance of serum MtCK activity in chronic hepatitis C patients without HCC. As a result, we have found that serum MtCK activity may be increased correlatively with the stage of liver fibrosis and hepatocellular damage, and that the increased serum MtCK activity is an independent risk for hepatocarcinogenesis, which could be the important information for physicians.

As MtCK is not naturally secreted from the cells, the active production of MtCK in a certain tissue or organ and its active release into the blood stream are assumed to be necessary for the increase in serum MtCK activity. Indeed, the increased uMtCK mRNA expression and the increased immunoreactivity for uMtCK were observed predominantly in hepatocytes of fibrotic livers in mice induced by bile duct ligation in our study, suggesting that the active production of uMtCK in fibrotic livers. Furthermore, the strong correlations between serum MtCK activity and serum levels of AST and ALT may suggest that serum MtCK activity is increased in association with hepatocellular damage, leading to the active release of MtCK from hepatocytes into the blood stream.

It is well known that HCV-related cirrhosis is associated with an extremely high risk of HCC development, with a reported annual incidence ranging between 3 and 8%,[4,21,22] indicating that advanced liver fibrosis is one of the strongest risk factors for HCC development in chronic hepatitis C patients. As our current results suggest that serum MtCK activity may be increased in association with the stage of liver fibrosis, the increased serum MtCK activity as a risk factor for hepatocarcinogenesis in chronic hepatitis C patients could be explained, at least in part, by the association between serum MtCK activity and liver fibrosis. In our study, higher serum MtCK activity but not elevated liver stiffness value was determined as a risk for HCC development on multivariate analysis. This finding may be explained by that liver stiffness value, being strongly correlated with serum MtCK

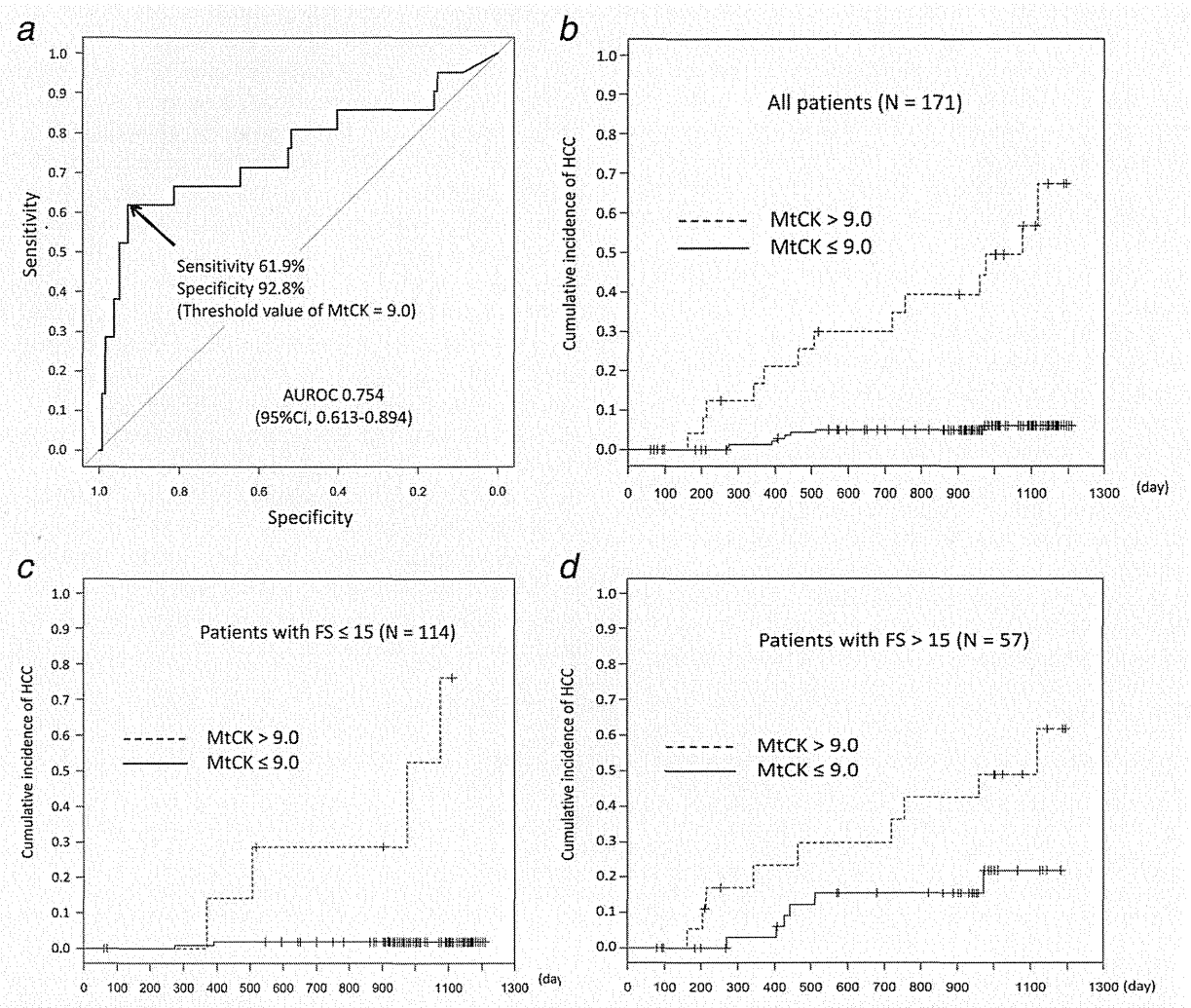

Figure 3. ROC curve showing the overall accuracy of serum MtCK activity for the prediction of HCC development and cumulative incidence of HCC subdivided according to serum MtCK activity in chronic hepatitis C patients. (*a*) ROC curve showing the overall accuracy of serum MtCK activity for the prediction of HCC development in chronic hepatitis C patients. The arrow identifies the best cutoff value (*i.e.*, 9.0 U/L) of serum MtCK activity. Then, cumulative incidence rates of HCC were estimated by the Kaplan–Meier method in all patients (*b*), in patients with liver stiffness value (LSV) of ≤15 kPa (*c*), and in patients with LSV of >15 kPa (*d*) subdivided according to their serum MtCK activity of 9.0 U/L. Serum MtCK activity of >9.0 U/L was a significantly higher risk for HCC development compared to those with serum MtCK of <9.0 U/L ($p < 0.001$) in all patient groups. Solid line, MtCK ≤ 9.0 U/L; dashed line, MtCK > 9.0 U/L.

activity as a predicting factor for liver fibrosis, was not retained as an independent risk for HCC development as a confounding factor. When evaluating this result, we should also bear in mind that another factor other than liver fibrosis may be responsible for the strong association between serum MtCK activity and HCC development. In this context, of interest is the evidence that the higher serum ALT levels were associated with the higher rate of HCC development[23] and HCC recurrence after the surgical treatment[24] in HCV-related cirrhosis, suggesting that the active hepatocellular damage may also be a risk for HCC development. Thus, the association between serum MtCK activity and hepatocellular damage, in addition to liver fibrosis, may explain the reason why serum MtCK activity was retained as an independent risk for hepatocarcinogenesis on multivariate analysis.

In our study, a significant association between serum MtCK activity and serum AFP levels was observed. As it is well known, serum AFP levels have been widely used as a serological marker for HCC[25] although the combination with other serological markers and imaging techniques is recommended to increase diagnostic accuracy.[26] However, elevated serum AFP levels are often observed in patients with chronic hepatitis C without HCC.[27–29] Although the mechanism(s) underlying this finding has not been fully understood yet, it was reported that serum AFP levels were independently associated with liver fibrosis and serum AST levels.[28,30] Thus, it

may be reasonable to assume that serum MtCK activity would behave similarly to serum AFP levels, both of which may be associated with liver fibrosis and hepatocellular damage. Indeed, in our study, both serum MtCK activity and serum AFP levels were retained as a risk for hepatocarcinogenesis, which may be in line with the evidence that the higher serum AFP levels were a risk for HCC development in cirrhotic patients.[31,32] Serum MtCK activity as a risk for HCC development should be further evaluated in comparison with serum AFP levels in a larger cohort with a variety of etiology.

As healthy liver tissue is known to be one of the few tissues that, in general, does not express detectable amounts of uMtCK,[33] uMtCK expression in the liver is assumed to be a sign of pathological development associated with, for example, ischemic–reperfusion injury[34] or tumor formation.[35] In agreement with this notion, in our study, serum MtCK activity was increased in association particularly with liver fibrosis and hepatocellular damage. Although a role of MtCK expression in pathological liver tissues remains to be elucidated, the evidence from CK gene transgenic mice, which showed that CK expression in the liver led to inhibition of apoptosis[36,37] and protection against hypoxia or endotoxin perfusion,[38–40] may suggest a protective role of MtCK expression in injured liver tissues. Indeed, MtCK has been assumed to be important for the energetics of oxidative tissues to control cellular energy homeostasis by building up a large pool of rapidly diffusing phosphocreatine for temporal and spatial buffering of ATP levels.[33] Hence, it is speculated that the increased MtCK activity may support active proliferation of the injured liver tissues to regenerate, which may ultimately lead to hepatocarcinogenesis as a result of enhanced proliferative activity as suggested previously.[32]

One of the limitations of our study is that serum MtCK activity was analyzed in a relatively small number of patients with chronic hepatitis C. In addition, the enrolled patients were at an older age (mean age, 68 years), which may be in line with the trend that the prevalence of older patients with chronic hepatitis C has been increasing in Japan.[41] In our study, as our cohort had a relatively narrow age distribution, age might not be retained as a risk for hepatocarcinogenesis. Nonetheless, serum MtCK activity as a risk for hepatocarcinogenesis should be further validated in a larger number of patients with other etiology, such as chronic hepatitis B or nonalcoholic steatohepatitis.

References

1. Ferlay J, Shin HR, Bray F, et al. Estimates of worldwide burden of cancer in 2008: GLOBOCAN 2008. *Int J Cancer* 2010;127:2893–917.
2. Llovet JM, Burroughs A, Bruix J. Hepatocellular carcinoma. *Lancet* 2003;362: 1907–17.
3. El-Serag HB. Epidemiology of hepatocellular carcinoma in USA. *Hepatol Res* 2007;37:S88–94.
4. Yoshida H, Shiratori Y, Moriyama M, et al. Interferon therapy reduces the risk for hepatocellular carcinoma: national surveillance program of cirrhotic and noncirrhotic patients with chronic hepatitis C in Japan. IHIT Study Group. Inhibition of Hepatocarcinogenesis by Interferon Therapy. *Ann Intern Med* 1999;131:174–81.
5. Bertino G, Di Carlo I, Ardiri A, et al. Systemic therapies in hepatocellular carcinoma: present and future. *Future Oncol* 2013;9:1533–48.
6. Biondi A, Malaguarnera G, Vacante M, et al. Elevated serum levels of Chromogranin A in hepatocellular carcinoma. *BMC Surg* 2012;12:S7.
7. Bertino G, Ardiri A, Malaguarnera M, et al. Hepatocellualar carcinoma serum markers. *Semin Oncol* 2012;39:410–33.
8. Soroida Y, Ohkawa R, Nakagawa H, et al. Increased activity of serum mitochondrial isoenzyme of creatine kinase in hepatocellular carcinoma patients predominantly with recurrence. *J Hepatol* 2012;57:330–36.
9. Uranbileg B, Enooku K, Soroida Y, et al. High ubiquitous mitochondrial creatine kinase expression in hepatocellular carcinoma denotes a poor prognosis with highly malignant potential. *Int J Cancer* 2013 Oct 15. doi: 10.1002/ijc.28547. [Epub ahead of print]
10. Kanemitsu F, Kawanishi I, Mizushima J, et al. Mitochondrial creatine kinase as a tumor-associated marker. *Clin Chim Acta* 1984;138:175–83.
11. Pratt R, Vallis LM, Lim CW, et al. Mitochondrial creatine kinase in cancer patients. *Pathology* 1987;19:162–65.
12. Qian XL, Li YQ, Gu F, et al. Overexpression of ubiquitous mitochondrial creatine kinase (uMtCK) accelerates tumor growth by inhibiting apoptosis of breast cancer cells and is associated with a poor prognosis in breast cancer patients. *Biochem Biophys Res Commun* 2012;427:60–66.
13. Patra S, Bera S, SinhaRoy S, et al. Progressive decrease of phosphocreatine, creatine and creatine kinase in skeletal muscle upon transformation to sarcoma. *FEBS J* 2008;275:3236–47.
14. Stein W, Bohner J, Renn W, et al. Macro creatine kinase type 2: results of a prospective study in hospitalized patients. *Clin Chem* 1985;31:1959–64.
15. Lee KN, Csako G, Bernhardt P, et al. Relevance of macro creatine kinase type 1 and type 2 isoenzymes to laboratory and clinical data. *Clin Chem* 1994;40:1278–83.
16. Hoshino T, Sakai Y, Yamashita K, et al. Development and performance of an enzyme immunoassay to detect creatine kinase isoenzyme MB activity using anti-mitochondrial creatine kinase monoclonal antibodies. *Scand J Clin Lab Invest* 2009;69:687–95.
17. Castera L, Vergniol J, Foucher J, et al. Prospective comparison of transient elastography, Fibrotest, APRI, and liver biopsy for the assessment of fibrosis in chronic hepatitis C. *Gastroenterology* 2005;128:343–50.
18. Kageyama Y, Ikeda H, Watanabe N, et al. Antagonism of sphingosine 1-phosphate receptor 2 causes a selective reduction of portal vein pressure in bile duct-ligated rodents. *Hepatology* 2012;56:1427–38.
19. Torzilli G, Minagawa M, Takayama T, et al. Accurate preoperative evaluation of liver mass lesions without fine-needle biopsy. *Hepatology* 1999;30:889–93.
20. Makuuchi M, Kokudo N, Arii S, et al. Development of evidence-based clinical guidelines for the diagnosis and treatment of hepatocellular carcinoma in Japan. *Hepatol Res* 2008;38:37–51.
21. Tsukuma H, Hiyama T, Tanaka S, et al. Risk factors for hepatocellular carcinoma among patients with chronic liver disease. *N Engl J Med* 1993; 328:1797–801.
22. Ikeda K, Saitoh S, Koida I, et al. A multivariate analysis of risk factors for hepatocellular carcinogenesis: a prospective observation of 795 patients with viral and alcoholic cirrhosis. *Hepatology* 1993;18:47–53.
23. Tarao K, Rino Y, Ohkawa S, et al. Association between high serum alanine aminotransferase levels and more rapid development and higher rate of incidence of hepatocellular carcinoma in patients with hepatitis C virus-associated cirrhosis. *Cancer* 1999;86:589–95.
24. Tarao K, Takemiya S, Tamai S, et al. Relationship between the recurrence of hepatocellular carcinoma (HCC) and serum alanine aminotransferase levels in hepatectomized patients with hepatitis C virus-associated cirrhosis and HCC. *Cancer* 1997; 79:688–94.
25. El-Serag HB, Marrero JA, Rudolph L, et al. Diagnosis and treatment of hepatocellular carcinoma. *Gastroenterology* 2008;134:1752–63.
26. Bertino G, Neri S, Bruno CM, et al. Diagnostic and prognostic value of alpha-fetoprotein, des-gamma-carboxy prothrombin and squamous cell carcinoma antigen immunoglobulin M complexes in hepatocellular carcinoma. *Minerva Med* 2011; 102:363–71.
27. Bayati N, Silverman AL, Gordon SC. Serum alpha-fetoprotein levels and liver histology in

patients with chronic hepatitis C. *Am J Gastroenterol* 1998;93:2452–56.
28. Goldstein NS, Blue DE, Hankin R, et al. Serum alpha-fetoprotein levels in patients with chronic hepatitis C. Relationships with serum alanine aminotransferase values, histologic activity index, and hepatocyte MIB-1 scores. *Am J Clin Pathol* 1999;111:811–16.
29. Chu CW, Hwang SJ, Luo JC, et al. Clinical, virologic, and pathologic significance of elevated serum alpha-fetoprotein levels in patients with chronic hepatitis C. *J Clin Gastroenterol* 2001;32:240–44.
30. Hu KQ, Kyulo NL, Lim N, et al. Clinical significance of elevated alpha-fetoprotein (AFP) in patients with chronic hepatitis C, but not hepatocellular carcinoma. *Am J Gastroenterol* 2004;99:860–65.
31. Oka H, Tamori A, Kuroki T, et al. Prospective study of alpha-fetoprotein in cirrhotic patients monitored for development of hepatocellular carcinoma. *Hepatology* 1994;19:61–66.
32. Sangiovanni A, Colombo E, Radaelli F, et al. Hepatocyte proliferation and risk of hepatocellular carcinoma in cirrhotic patients. *Am J Gastroenterol* 2001;96:1575–80.
33. Schlattner U, Tokarska-Schlattner M, Wallimann T. Mitochondrial creatine kinase in human health and disease. *Biochim Biophys Acta* 2006;1762:164–80.
34. Vaubourdolle M, Chazouilleres O, Poupon R, et al. Creatine kinase-BB: a marker of liver sinusoidal damage in ischemia-reperfusion. *Hepatology* 1993;17:423–28.
35. Kanemitsu F, Kawanishi I, Mizushima J. A new creatine kinase found in mitochondrial extracts from malignant liver tissue. *Clin Chim Acta* 1983;128:233–40.
36. Dolder M, Walzel B, Speer O, et al. Inhibition of the mitochondrial permeability transition by creatine kinase substrates. Requirement for microcompartmentation. *J Biol Chem* 2003;278:17760–66.
37. Hatano E, Tanaka A, Kanazawa A, et al. Inhibition of tumor necrosis factor-induced apoptosis in transgenic mouse liver expressing creatine kinase. *Liver Int* 2004;24:384–93.
38. Miller K, Halow J, Koretsky AP. Phosphocreatine protects transgenic mouse liver expressing creatine kinase from hypoxia and ischemia. *Am J Physiol* 1993;265:C1544–51.
39. Hatano E, Tanaka A, Iwata S, et al. Induction of endotoxin tolerance in transgenic mouse liver expressing creatine kinase. *Hepatology* 1996;24:663–69.
40. Miller K, Sharer K, Suhan J, et al. Expression of functional mitochondrial creatine kinase in liver of transgenic mice. *Am J Physiol* 1997;272:C1193–202.
41. Tanaka Y, Hanada K, Mizokami M, et al. A comparison of the molecular clock of hepatitis C virus in the United States and Japan predicts that hepatocellular carcinoma incidence in the United States will increase over the next two decades. *Proc Natl Acad Sci USA* 2002;99:15584–89.

Loss of liver E-cadherin induces sclerosing cholangitis and promotes carcinogenesis

Hayato Nakagawa[a,b,1,2], Yohko Hikiba[c,1], Yoshihiro Hirata[a], Joan Font-Burgada[b], Kei Sakamoto[c], Yoku Hayakawa[a], Koji Taniguchi[b], Atsushi Umemura[b], Hiroto Kinoshita[a], Kosuke Sakitani[a,c], Yuji Nishikawa[d], Kenji Hirano[a], Tsuneo Ikenoue[e], Hideaki Ijichi[a], Debanjan Dhar[b], Wataru Shibata[f], Masao Akanuma[c], Kazuhiko Koike[a], Michael Karin[b,2], and Shin Maeda[f,2]

[a]Department of Gastroenterology, University of Tokyo, Bunkyo-ku, Tokyo 113-8655, Japan; [b]Laboratory of Gene Regulation and Signal Transduction, Departments of Pharmacology and Pathology, School of Medicine, University of California, San Diego, La Jolla, CA 92093; [c]Division of Gastroenterology, Institute for Adult Diseases, Asahi Life Foundation, Chuo-ku, Tokyo 103-0002, Japan; [d]Division of Tumor Pathology, Department of Pathology, Asahikawa Medical University, Higashi Asahikawa, Hokkaido 078-8510, Japan; [e]Division of Clinical Genome Research, Institute of Medical Science, University of Tokyo, Tokyo 108-8639, Japan; and [f]Department of Gastroenterology, Yokohama City University, Kanazawa-ku, Yokohama 236-0004, Japan

Contributed by Michael Karin, December 6, 2013 (sent for review November 4, 2013)

E-cadherin is an important adhesion molecule whose loss is associated with progression and poor prognosis of liver cancer. However, it is unclear whether the loss of E-cadherin is a real culprit or a bystander in liver cancer progression. In addition, the precise role of E-cadherin in maintaining liver homeostasis is also still unknown, especially in vivo. Here we demonstrate that liver-specific E-cadherin knockout mice develop spontaneous periportal inflammation via an impaired intrahepatic biliary network, as well as periductal fibrosis, which resembles primary sclerosing cholangitis. Inducible gene knockout studies identified E-cadherin loss in biliary epithelial cells as a causal factor of cholangitis induction. Furthermore, a few of the E-cadherin knockout mice developed spontaneous liver cancer. When knockout of E-cadherin is combined with Ras activation or chemical carcinogen administration, E-cadherin knockout mice display markedly accelerated carcinogenesis and an invasive phenotype associated with epithelial–mesenchymal transition, up-regulation of stem cell markers, and elevated ERK activation. Also in human hepatocellular carcinoma, E-cadherin loss correlates with increased expression of mesenchymal and stem cell markers, and silencing of E-cadherin in hepatocellular carcinoma cell lines causes epithelial–mesenchymal transition and increased invasiveness, suggesting that E-cadherin loss can be a causal factor of these phenotypes. Thus, E-cadherin plays critical roles in maintaining homeostasis and suppressing carcinogenesis in the liver.

liver progenitor cell | cholangiocellular carcinoma | mixed type tumor

E-cadherin is an important adhesion molecule, and not only establishes the core of the epithelial adherens junction with neighboring cells but also participates in intracellular signaling (1, 2). E-cadherin knockout mice die early during embryogenesis due to failed blastocyst and trophectoderm formation (3). Conditional knockout of E-cadherin in skin impairs an epidermal water-barrier function that leads to perinatal lethality (4). In addition, E-cadherin deletion in the differentiating alveolar epithelial cells of mammary gland results in an impaired differentiation program during lactation (5). Thus, although E-cadherin is a key regulator of embryonic development and tissue homeostasis, its role varies depending on the organ. Adult liver parenchyma consists of two types of hepatic epithelial cells, hepatocytes and biliary epithelial cells (BECs), and both cell types express E-cadherin localizing at the junctional complex (6). However, the precise functional role of E-cadherin in the liver is still unknown, especially in vivo.

Dysregulation of E-cadherin also contributes to cancer progression. In fact, mutation or decreased expression of E-cadherin is associated with malignant progression in various cancers, such as gastric, breast, and skin cancer (7). Also in human liver cancers, such as hepatocellular carcinoma (HCC) and cholangiocellular carcinoma (CCC), E-cadherin expression is decreased by 20–60% and is associated with higher histological grade, invasiveness, and poor prognosis (8–10). These findings suggest that E-cadherin may be a tumor suppressor in liver tumorigenesis. However, down-regulation of E-cadherin in liver cancer is caused by several mechanisms, including loss of heterozygosity, methylation of the E-cadherin promoter region, transcriptional repressors, and gene-silencing microRNAs (miRs) (8, 11–13). Transcriptional repressors such as Snail, Slug, and Twist, as well as miR-9, play an important role in induction of the epithelial–mesenchymal transition (EMT), which is a major cancer progression-mediating process. E-cadherin is a major target of these factors; however, they also control other EMT-inducing molecules involved in junctional complexes, intermediate filament networks, and the actin cytoskeleton (14). Therefore, it is unclear whether the loss of E-cadherin is a real culprit or a bystander in EMT induction and liver cancer progression. In addition, expression of E-cadherin can be increased during the early stages of HCC (11), and it has been suggested that preservation of E-cadherin expression may be beneficial for tumor growth, invasion, and metastasis (11, 15). Thus, here we characterize the role of E-cadherin in liver homeostasis and carcinogenesis in vivo using liver-specific E-cadherin knockout mice.

Results

Spontaneous Portal Inflammation and Periductal Fibrosis in *CDH1*$^{\Delta L}$ Mice. Liver-specific E-cadherin knockout mice ($CDH1^{\Delta L}$) were generated by crossing CDH1 flox/flox ($CDH1^{F/F}$) mice with

Significance

The precise roles of E-cadherin in the liver and liver carcinogenesis are still unknown. Here we show that mice lacking E-cadherin in the liver develop spontaneous periportal inflammation via an impaired intrahepatic biliary network, as well as periductal fibrosis, which resembles primary sclerosing cholangitis. Inducible gene knockout studies identified E-cadherin loss in biliary epithelial cells as a causal factor of cholangitis induction, and dysregulated E-cadherin expression was also seen in patients with primary sclerosing cholangitis. E-cadherin loss also significantly accelerates genetically and chemically engineered liver cancer through epithelial–mesenchymal transition, up-regulation of stem cell markers, and ERK activation. Thus, E-cadherin plays critical roles in maintaining homeostasis and suppressing carcinogenesis in the liver.

Author contributions: H.N., J.F.-B., and S.M. designed research; H.N., Y. Hikiba, Y. Hirata, J.F.-B., K. Sakamoto, Y. Hayakawa, K.T., A.U., H.K., K. Sakitani, K.H., T.I., H.I., D.D., W.S., M.A., and S.M. performed research; H.N., Y.N., K.K., and S.M. analyzed data; and H.N., J.F.-B., M.K., and S.M. wrote the paper.

The authors declare no conflict of interest.

[1]H.N. and Y. Hikiba contributed equally to this work.

[2]To whom correspondence may be addressed. E-mail: hayaton0120@gmail.com, karinoffice@ucsd.edu, or smaeda@med.yokohama-cu.ac.jp.

This article contains supporting information online at www.pnas.org/lookup/suppl/doi:10.1073/pnas.1322731111/-/DCSupplemental.

albumin-Cre transgenic (*Alb-Cre*) mice. Immunohistochemistry (IHC) and immunofluorescence (IF) revealed that E-cadherin was expressed in the membrane of hepatocytes, especially in zone 1, and in the interlobular BECs in 1-mo-old $CDH1^{F/F}$ mice, whereas it was completely absent from both hepatocytes and interlobular BECs in $CDH1^{\Delta L}$ mice of the same age (Fig. 1*A* and Fig. S1*A*). On the other hand, E-cadherin expression was preserved in the large bile duct that is near the common bile duct (Fig. S1*B*). These results are consistent with recent reports of Cre expression in hepatocytes and interlobular BECs of *Alb-Cre* mice (16).

The histology of the liver appeared almost normal in 1-mo-old $CDH1^{\Delta L}$ mice (Fig. 1*B*). However, at 2 mo of age, $CDH1^{\Delta L}$ mice spontaneously developed periportal inflammation, followed by periductal fibrosis resembling primary sclerosing cholangitis (PSC) at 8 mo of age (Fig. 1 *B* and *C*). IHC for α-smooth muscle actin confirmed activation of fibroblasts in the periductal area (Fig. 1*D*). These histological changes were not seen in $CDH1^{F/F}$ mice. As is the case in cholestasis, serum levels of total bile acid and alkaline phosphatase (ALP) were significantly elevated in $CDH1^{\Delta L}$ mice compared with $CDH1^{F/F}$ mice (Fig. 1*E*). Terminal deoxynucleotidyl transferase-mediated dUTP nick-end labeling (TUNEL) staining revealed that TUNEL-positive nonhepatocyte cells were noticeable in the periportal area in $CDH1^{\Delta L}$ mice (Fig. S1*C*). Although these cells were mostly $CD45^+$ leukocytes, they also contained K19-positive BECs, which were completely absent in $CDH1^{F/F}$ mice (Fig. S1 *D*–*F*). In comparison, there were no significant differences in serum alanine aminotransferase (ALT) and the number of TUNEL-positive hepatocytes between $CDH1^{F/F}$ mice and $CDH1^{\Delta L}$ mice other than a small increase of TUNEL-positive hepatocytes in 2-mo-old $CDH1^{\Delta L}$ mice (Fig. 1*E* and Fig. S1*G*). Hence, BEC injury could be one of the main factors contributing to development of periductal fibrosis.

Next, we postulated that cholestatic liver injury and periportal inflammation might be caused by disruption of the junction complex due to loss of E-cadherin. However, electron microscopy revealed no obvious morphological abnormalities in the adherens junctions, tight junctions, desmosomes, or bile canaliculi in 2-mo-old $CDH1^{\Delta L}$ mice (Fig. S1*H*). To functionally analyze the bile transport system, we injected fluorescent-labeled bile acid into the tail vein of 2-mo-old mice. Fifteen minutes after the injection, we could see clear canalicular staining in $CDH1^{F/F}$ mouse liver and smooth transport of bile acid into the bile duct lumen. In contrast, the canalicular staining pattern in $CDH1^{\Delta L}$ mice was very fuzzy, particularly in zone 1, and bile acid had not yet reached the bile duct lumen (Fig. 1*E*). These results suggest that the intrahepatic biliary network may be functionally impaired in $CDH1^{\Delta L}$ mice, which could lead to cholestatic liver injury and subsequent inflammation.

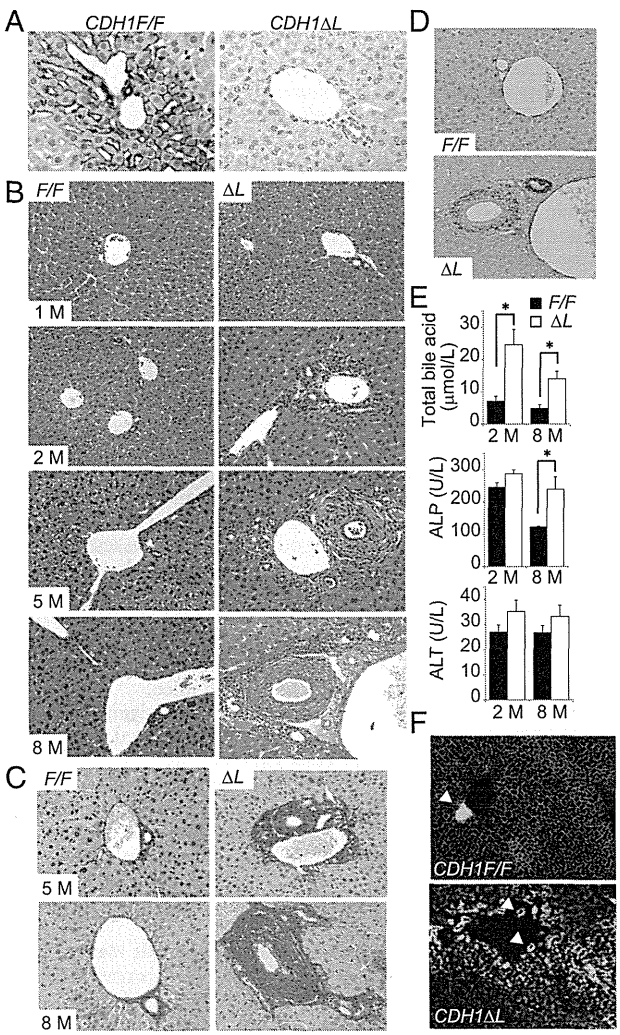

Fig. 1. Spontaneous development of portal inflammation and periductal fibrosis in $CDH1^{\Delta L}$ mice. (*A*) Analysis of E-cadherin expression by IHC of liver sections (×200) obtained from 1-mo-old $CDH1^{F/F}$ and $CDH1^{\Delta L}$ mice. (*B*) H&E staining of 1-, 2-, 5-, and 8-mo-old mice (representative images, ×200). (*C*) Sirius red staining in 5- and 8-mo-old mice (×200). (*D*) IHC of α-smooth muscle actin in 8-mo-old mice (×200). (*E*) Serum levels of total bile acid, ALP, and ALT in 2- and 8-mo-old mice. Results are means ± SEM (n = 5–7 per group; *$P < 0.05$). (*F*) Functional analysis of the bile transport system in 2-mo-old mice injected with fluorescent-labeled bile acid in the tail vein for 15 min followed by analysis of staining in the bile canaliculi (×200). Arrowheads indicate interlobular bile duct lumen (n = 3 per group).

Loss of E-Cadherin in BECs Rather than Hepatocytes Is a Causal Factor of Cholangitis Induction. To distinguish the function of E-cadherin in hepatocytes and BECs maintaining liver homeostasis, we generated two different models of E-cadherin deletion in the liver (Fig. 2*A*). First, to delete E-cadherin only in hepatocytes, we i.v. injected 5-wk-old $CDH1^{F/F}$ mice with adenovirus expressing Cre-recombinase (Ad-Cre) or control adenovirus (Ad-Cont) (17). We confirmed that this method induced Cre-loxP recombination in 73.0 ± 4.2% (mean ± SD) of hepatocytes but no recombination in BECs at 1 wk after injection using Rosa26-lox-stop-lox-YFP mice (Fig. S2*A*). Although E-cadherin expression was still reduced significantly in Ad-Cre–injected $CDH1^{F/F}$ mice at 8 wk after injection (Fig. S2 *B* and *C*), there was no apparent periportal inflammation (Fig. 2*B*). Next, to delete E-cadherin only in BECs, we crossed $CDH1^{F/F}$ mice with $K19^{CreERT}$ mice in which tamoxifen (TAM)-inducible Cre ERT was knocked into the endogenous K19 locus ($CDH1^{F/F}/K19^{CreERT}$) (18). According to the previous study, which showed relatively low efficacy of recombination in BECs, we injected TAM twice, at 5 and 9 wk after birth. One week after the first TAM injection into $CDH1^{F/F}/K19^{CreERT}$ mice, E-cadherin expression was deleted in 31.2 ± 7.2% of K19-positive BECs, whereas E-cadherin in the hepatocytes was well-preserved (Fig. S2*D*). Eight weeks after the first TAM injection, four of eight $CDH1^{F/F}/K19^{CreERT}$ mice revealed significant periportal inflammation as seen in $CDH1^{\Delta L}$ mice (Fig. 2*C*). Although the rate of E-cadherin loss in BECs varied widely in TAM-injected $CDH1^{F/F}/K19^{CreERT}$ mice at this point (25.5 ± 17.1%), bile ducts with strong inflammation tended to show high rates of E-cadherin deletion (Fig. 2*D* and Fig. S2*E*). Thus, loss of E-cadherin in BECs rather than hepatocytes is a causal factor of periportal inflammation. Furthermore, in human liver samples, a clear membranous pattern of E-cadherin expression in the epithelial cells of medium-size bile ducts was seen in normal liver, whereas it mostly disappeared, with only fragmented cytoplasmic expression, in four of seven PSC samples (Fig. 2*E*). In contrast, E-cadherin

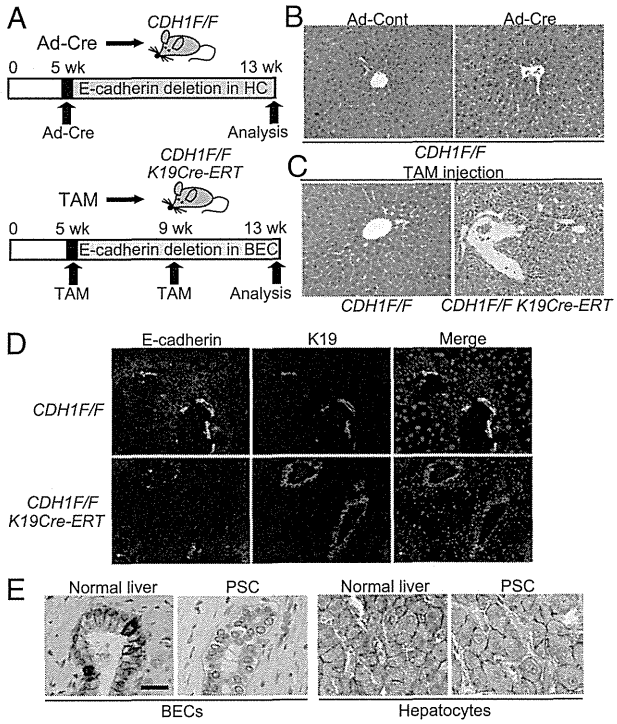

Fig. 2. Loss of E-cadherin in BECs rather than hepatocytes is a causal factor in periportal inflammation. (*A*) Experimental protocol of E-cadherin deletion in hepatocytes (HC) (*Upper*) or BECs (*Lower*). (*B*) H&E staining of liver sections from Ad-Cont– or Ad-Cre–injected $CDH1^{F/F}$ mice at 8 wk after adenovirus injection (×200). (*C* and *D*) Histological analyses of $CDH1^{F/F}$ and $CDH1^{F/F}$/$K19^{CreERT}$ mice at 8 wk after TAM injection. H&E staining (×200) (*C*) and double IF staining of E-cadherin (green) and K19 (red) (×400) (*D*). (*E*) IHC of E-cadherin in human normal liver and PSC samples ($n = 7$). (Scale bar, 20 μm.)

expression in hepatocytes was well-preserved in all samples. Based on these data, abnormality of E-cadherin expression in BECs might contribute to the pathogenesis of PSC.

Ductular Reaction in $CDH1^{\Delta L}$ Mice. To further characterize $CDH1^{\Delta L}$ mice, we conducted cDNA microarray analysis using whole-liver samples from young (2-mo-old) and aged (11-mo-old) $CDH1^{F/F}$ and $CDH1^{\Delta L}$ mice. Interestingly, expression of progenitor cell markers such as Sox9, CD44, and Epcam, as well as inflammatory cytokines and chemokines, was up-regulated in both young and aged $CDH1^{\Delta L}$ mice compared with age-matched $CDH1^{F/F}$ mice (Fig. S3*A*). The microarray results were confirmed by IHC of these markers, and we found numerous primitive duct cells expressing progenitor cell markers, the so-called ductular reaction, in the periportal area (Fig. S3*B*). IHC of Ki67 revealed significant ongoing proliferation of these primitive duct cells but not hepatocytes in $CDH1^{\Delta L}$ mice (Fig. S3 *B* and *C*). Inflammatory cytokines have been implicated in hepatic progenitor cell induction (19), and $CDH1^{\Delta L}$ mice revealed infiltration of numerous F4/80-positive macrophages in the periportal area (Fig. S3*D*). Macrophage depletion by liposomal clodronate remarkably decreased the expression of interleukin 6, which is one of the major progenitor cells inducing cytokines (19), and subsequently reduced the ductular reaction (Fig. S3 *E*–*G*). Thus, the ductular reaction was due, in part, to macrophage-mediated inflammatory response.

Loss of E-Cadherin Accelerates Liver Tumorigenesis. A few of the male $CDH1^{\Delta L}$ mice (2/12, 16.7%) spontaneously developed liver tumors at 11 mo of age (Fig. S4 *A* and *B*). Most of the tumors were α-fetoprotein (AFP)–positive HCC, and negative for E-cadherin (Fig. S4 *C*–*E*). However, the tumor incidence rate in $CDH1^{\Delta L}$ mice was too low to investigate the detailed mechanism of hepatocarcinogenesis. Because Ras signaling is frequently activated in human HCC, we generated liver-specific active *Kras*-expressing $CDH1^{\Delta L}$ mice (*Kras*/$CDH1^{\Delta L}$) by crossing $CDH1^{\Delta L}$ mice with $Kras^{G12D}$ conditional knockin (*LSL-*$Kras^{G12D}$) mice. Strikingly, all male *Kras*/$CDH1^{\Delta L}$ mice developed multiple liver tumors at 8 mo of age ($n = 10$), whereas only 4 of 10 male *Alb-Cre*/*LSL-*$Kras^{G12D}$/*CDH1* wild-type mice (*Kras*/$CDH1^{+/+}$) developed a few macroscopically visible small tumors at the same age (Fig. 3*A*). Quantitative analyses also showed significant acceleration of liver tumorigenesis by E-cadherin loss (Fig. 3*B*). We confirmed the absence of E-cadherin in both nontumor and tumor tissue in *Kras*/$CDH1^{\Delta L}$ mice (Fig. 3*C*). Most of the tumors arising in *Kras*/$CDH1^{\Delta L}$ mice were AFP-positive HCC and ranged from the typical trabecular type to a poorly differentiated type (Fig. 3*D*). Importantly, CCC and mixed-type HCC/CCC tumors were also seen in 10% and 40% of *Kras*/$CDH1^{\Delta L}$ mice, respectively (Fig. 3*D*). On the other hand, tumors in *Kras*/$CDH1^{+/+}$ mice were mostly AFP-negative dysplastic nodules or well-differentiated HCC (Fig. 3*D*). These results suggest that loss of E-cadherin cooperates with Ras signaling in liver cancer development.

Next, we assessed activation of extracellular signal-regulated kinase (ERK), which is a major downstream transducer of Ras, in nontumor tissue. ERK phosphorylation was almost undetectable by IHC in $CDH1^{F/F}$ mouse liver and faintly detected in periportal hepatocytes of $CDH1^{\Delta L}$ mice. *Kras*/$CDH1^{+/+}$ mice had diffuse ERK phosphorylation that was further increased in *Kras*/$CDH1^{\Delta L}$ mice (Fig. 3*E*). These findings were confirmed by Western blotting (WB) (Fig. S5*A*). To eliminate the influence of environmental factors on ERK activation, we isolated primary hepatocytes from $CDH1^{F/F}$, *LSL-Kras*/$CDH1^{+/+}$, and *LSL-KRas*/$CDH1^{F/F}$ mice (all Cre-negative), and then induced gene recombination by Ad-Cre infection. Ad-Cre efficiently induced gene recombination, and Ras activation and E-cadherin loss cooperatively increased ERK phosphorylation (Fig. 3*F*). This finding was confirmed in an immortalized human normal hepatocyte (20) by transfection of active Ras and knockdown of E-cadherin (Fig. S5*B*). E-cadherin was reported to inhibit the phosphorylation of several receptor tyrosine kinases (RTKs) (21), and phospho-RTK array analysis revealed that Ad-Cre–mediated E-cadherin deletion significantly increased only epithelial growth factor receptor (EGFR) phosphorylation (Fig. S5*C*). Thus, the cooperative activation of ERK by Ras and E-cadherin loss-induced EGFR phosphorylation may explain the accelerated carcinogenesis in *Kras*/$CDH1^{\Delta L}$ mice.

Furthermore, the ductular reaction was also significantly induced in *Kras*/$CDH1^{\Delta L}$ mice, likely due to increased ERK activation in the primitive duct cells (Fig. 3*G* and Fig. S5*D*). In addition to quantitative change, morphology of proliferating duct cells in *Kras*/$CDH1^{\Delta L}$ mice was sometimes dysplastic compared with that in $CDH1^{\Delta L}$ mice (Fig. 3*H*). These findings, along with CCC and mixed-type tumors, suggested that some tumors in *Kras*/$CDH1^{\Delta L}$ mice might originate from primitive duct cells, including bipotential progenitor cells induced by inflammation.

Spontaneous EMT, Vascular Invasion, and Intrahepatic Metastasis in *Kras*/$CDH1^{\Delta L}$ Tumors. EMT is considered a key process driving tumor invasiveness, and loss of E-cadherin expression is a hallmark of EMT (14). However, whether loss of E-cadherin is a consequence or a cause of EMT remains controversial. Importantly, in some tumors arising in *Kras*/$CDH1^{\Delta L}$ mice, HCC cells gradually transformed into fibroblast-like cells, and these cells are positive for both the HCC marker AFP and the mesenchymal marker vimentin, indicating that spontaneous EMT occurred in the tumors of these mice (Fig. 4 *A* and *B*). As expected, these cells were negative for E-cadherin (Fig. 4*B*). EMT was shown to be associated with a gain of stem cell properties (22). Indeed, evident expression of stem cell markers CD44 and Sox9 was seen in tumor cells undergoing EMT (Fig. 4*B*). We also found several tiny nodular lesions near the large

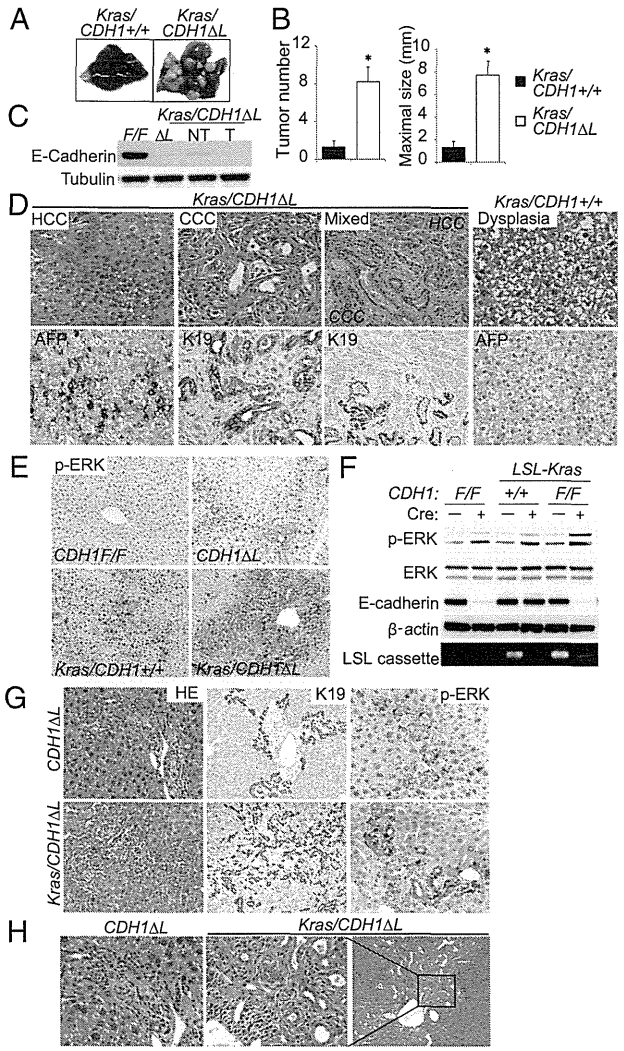

Fig. 3. Loss of E-cadherin cooperates with Ras activation in liver cancer development. (*A*) Representative images of the liver from 8-mo-old *Kras/CDH1*$^{+/+}$ and *Kras/CDH1*$^{\Delta L}$ mice. (*B*) Bar graphs of tumor number and maximal tumor size in each mouse are shown. Data are means ± SEM ($n = 10$ per group; *$P < 0.05$). (*C*) WB analysis of E-cadherin expression in nontumor (NT) and tumor (T) tissues in *Kras/CDH1*$^{\Delta L}$ mice. (*D*) H&E staining and IHC of AFP and K19 of tumors from *Kras/CDH1*$^{\Delta L}$ and *Kras/CDH1*$^{+/+}$ mice (mixed, ×200; others, ×400). (*E*) IHC analysis of ERK phosphorylation in nontumor areas of 8-mo-old mouse livers (×200). (*F*) Primary hepatocytes isolated from *CDH1*$^{F/F}$, *LSL-Kras*, and *Kras/CDH1*$^{F/F}$ mice were infected with Ad-Cont or Ad-Cre. The indicated proteins were assessed by WB 48 h after infection. Cre-mediated recombination of the *LSL-Kras* allele (deletion of LSL cassette) was confirmed by PCR. (*G*) Ductular reaction assessment by H&E and IHC of K19 and ERK phosphorylation in primitive duct cells in 8-mo-old mice (H&E and K19, ×200; p-ERK, ×400). (*H*) H&E staining of the ductular reaction with dysplastic change in *Kras/CDH1*$^{\Delta L}$ mice (*Right*, ×100; *Left* and *Center*, ×400).

tumors undergoing EMT. Despite their small size, these lesions resembled the adjacent larger tumor in that they were strongly positive for vimentin, CD44, and Sox9, suggesting that they might represent intrahepatic metastasis (Fig. 4*C*). However, although tumor cells frequently invaded the central vein lumen in *Kras/CDH1*$^{\Delta L}$ mice (Fig. 4*D*), we could not find any apparent extrahepatic metastasis in any tissues, including the lymph nodes.

Loss of E-cadherin has been reported to induce β-catenin nuclear translocation that can promote carcinogenesis (23). Although the β-catenin expression was increased in the cancer cell membrane in *Kras/CDH1*$^{\Delta L}$ mice, we could not detect any nuclear translocation in either nontumor or tumor areas (Fig. S6*A*). In addition, E-cadherin knockdown in HCC cell lines did not induce significant β-catenin nuclear translocation (Fig. S6*B*). Thus, this mechanism does not play a major role in enhanced carcinogenesis by loss of E-cadherin in the liver.

Loss of E-Cadherin Promotes Chemically Induced HCC. To further examine the tumor-suppressive role of E-cadherin, *CDH1*$^{F/F}$ mice and *CDH1*$^{\Delta L}$ mice were injected with diethylnitrosamine (DEN) on postnatal day 14 (20, 24). After 8 mo, *CDH1*$^{\Delta L}$ mice had significantly increased number and size of liver tumors and developed histologically more advanced HCC compared with *CDH1*$^{F/F}$ mice (Fig. S7 *A* and *B*). As seen in *Kras/CDH1*$^{\Delta L}$ mice, strong ERK phosphorylation was seen in tumors of DEN-treated *CDH1*$^{\Delta L}$ mice (Fig. S7*C*). In addition, although an obvious fibroblast-like morphological change was not seen, some tumors in *CDH1*$^{\Delta L}$ mice strongly expressed CD44 and vimentin, whereas very few tumors in *CDH1*$^{F/F}$ mice expressed these markers (Fig. S7*D*). This confirmed that loss of E-cadherin enhances activation of ERK and expression of stem cell and EMT markers in a chemically induced HCC model.

Correlating E-Cadherin Loss with Mesenchymal and Stem Cell Markers in Human HCC. To investigate whether E-cadherin loss correlates with mesenchymal and stem cell markers in human HCC, we examined the expression of E-cadherin, CD44, and vimentin in human HCC cell lines. There were significant inverse correlations, particularly between E-cadherin and CD44 (Fig. 5*A*). Among these cell lines, we chose three that expressed E-cadherin, Hep3B, HuH7, and Alexander, and assessed the effect of E-cadherin knockdown with siRNA. After 6 d of E-cadherin knockdown, all three cell lines exhibited elevated expression of mesenchymal markers such as N-cadherin and vimentin and underwent morphological changes that resulted in an elongated mesenchymal-like appearance (Fig. 5 *B* and *C*). In addition, invasion capacity was significantly increased by E-cadherin knockdown (Fig. 5*D*), suggesting that loss of E-cadherin can be a causal factor of EMT and invasive phenotype of HCC.

Furthermore, the expression of stem cell markers such as CD44 and Sox9 were also increased upon E-cadherin knockdown in Hep3B cells (Fig. 5*B*), as seen in mouse HCC models. However, HuH7 and Alexander cells did not show any significant changes in stem cell markers upon E-cadherin knockdown (Fig. 5*B*). As shown in microarray data (Fig. S3*A*), various inflammatory cytokines and chemokines were up-regulated in *CDH1*$^{\Delta L}$ mouse livers in vivo. Interestingly, tumor necrosis factor α (TNF-α) stimulation significantly increased CD44 expression in E-cadherin–knocked down HuH7 cells but not in control cells (Fig. 5*E*). In E-cadherin–knocked down Alexander cells, not TNF-α alone but TNF-α in combination with transforming growth factor β (TGF-β) and hepatocyte growth factor (HGF) significantly increased CD44 expression (Fig. 5*E*). These findings suggest that loss of E-cadherin can up-regulate CD44 expression cooperatively with the inflammatory environment.

E-cadherin knockdown in Hep3B and HuH7 cells increased expression of Snail (Fig. 5*B*), which is an upstream transcriptional repressor of E-cadherin that plays important roles in EMT induction. Also in vivo, tumor cells undergoing EMT in *Kras/CDH1*$^{\Delta L}$ mice strongly expressed Snail (Fig. S8*A*). Additional knockdown of Snail in Hep3B cells suppressed up-regulation of mesenchymal and stem cell markers caused by E-cadherin knockdown (Fig. 5*F*), suggesting that Snail may link E-cadherin loss to EMT.

Finally, we investigated the expression of E-cadherin, CD44, and vimentin using a human HCC tissue array. Expression of E-cadherin tended to be lost in advanced-stage HCC (percentage of E-cadherin loss: 33.3% in stage I/II and 55.6% in stage III; $P = 0.088$). CD44 and vimentin expression exhibited significant inverse correlations with E-cadherin expression (Fig. 5*G*).

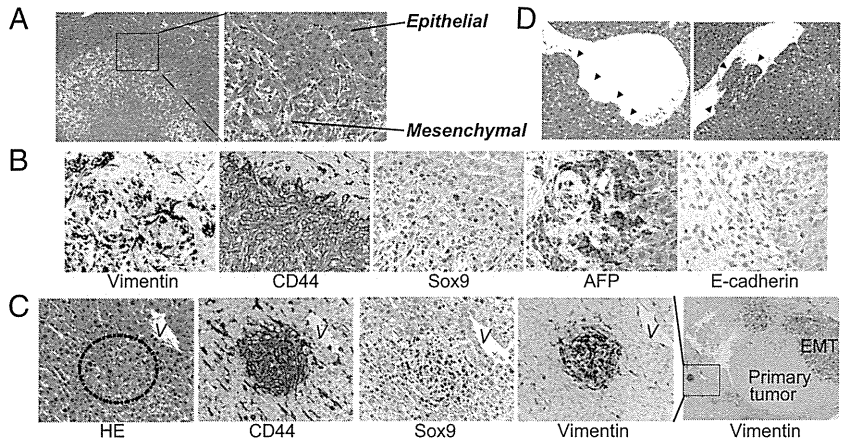

Fig. 4. Spontaneous epithelial–mesenchymal transition in tumors of *Kras/CDH1*$^{\Delta L}$ mice. (*A*) H&E staining of tumors from 8-mo-old *Kras/CDH1*$^{\Delta L}$ mice in which HCC cells gradually undergo an EMT-like morphological change (*Right*, ×400; *Left*, ×100). (*B*) Expression of the indicated proteins was assessed by IHC using serial sections (×200). (*C*) Intrahepatic metastasis-like lesions were seen near the large tumors undergoing EMT. Expression of EMT and stem cell markers in tiny nodular lesions was assessed by IHC using serial sections. V, vein near the lesion (*Right*, ×50; others, ×400). (*D*) H&E staining of tumor cell invasion into the central vein (×400). Arrowheads indicate invading cells.

Discussion

This study shows that E-cadherin plays critical roles in maintaining liver homeostasis. Although we assumed that periportal inflammation in *CDH1*$^{\Delta L}$ mice might be caused by disruption of the junction complex, electron microscopy showed no morphological abnormalities. This is consistent with a previous report (25). However, our functional analysis of the bile transport system using fluorescent-labeled bile acid showed impaired bile acid flow around zone 1. E-cadherin deletion in BECs by crossing *CDH1*$^{F/F}$ mice with *K19*^{CreERT} mice also triggered periportal inflammation similar to that seen in *CDH1*$^{\Delta L}$ mice. Therefore, loss of E-cadherin, especially in the intrahepatic bile duct epithelium, functionally impairs biliary flow, and subsequently induces cholestatic liver injury and sclerosing cholangitis. Our analysis of human PSC samples showed dysregulated E-cadherin expression in BECs, and another group also reported similar findings (26). Thus, abnormality of E-cadherin expression in BECs might contribute to the pathogenesis of PSC. Of note, PSC is well-known as an extraintestinal manifestation of ulcerative colitis (UC), and a recent genome-wide association study showed that single-nucleotide polymorphism in the CDH1 gene was associated with susceptibility to UC (27). Combined with our finding, impaired function of E-cadherin may be a common factor of these coexisting diseases.

Our data also suggest that E-cadherin is a tumor suppressor in the liver. A few *CDH1*$^{\Delta L}$ mice develop spontaneous HCC, and when knockout of E-cadherin is combined with Ras activation or chemical carcinogen administration, *CDH1*$^{\Delta L}$ mice display markedly accelerated carcinogenesis and an invasive phenotype. Although it has not been clear whether the loss of E-cadherin is a consequence or a cause of EMT, we have definitively demonstrated its causal role in vivo and in vitro. Recent reports have established a direct link between EMT and a gain of stem/progenitor cell properties (22), which is supported by our mouse models because tumor cells undergoing EMT clearly expressed stem cell markers. The expression of stem cell markers such as CD44 and Sox9 has been reported to be associated with poor prognosis in patients with HCC (28, 29). Interestingly, E-cadherin

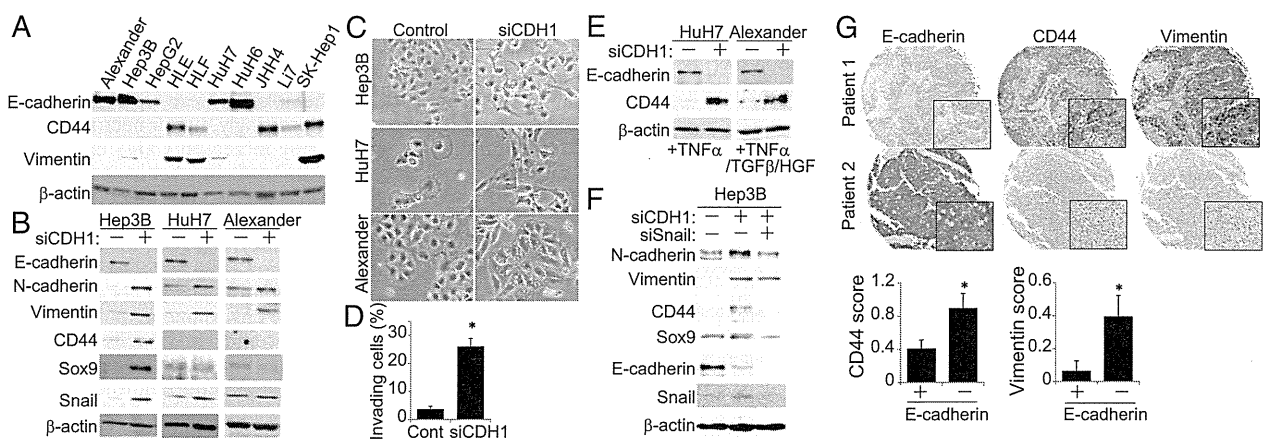

Fig. 5. Correlating E-cadherin loss with mesenchymal and stem cell markers in human HCC. (*A*) WB analysis of the indicated proteins in human HCC cell lines. (*B* and *C*) Effect of E-cadherin knockdown on human HCC cell lines. Expression levels of the indicated proteins (*B*) and morphological changes (*C*) in HCC cell lines 6 d after transfection with E-cadherin siRNA or controls. (*D*) Invasion capacity was assessed by invasion assay using Alexander cells. Bars show the percentages of invaded cells ($n = 3$). Data are means ± SD; $^*P < 0.05$. (*E*) The effect of E-cadherin knockdown on CD44 expression upon cytokine and/or growth factor stimulation in HuH7 and Alexander cells. Two days after transfection with E-cadherin or control siRNA, cells were stimulated with the indicated cytokines and/or growth factors (10 ng/mL TNF-α, 10 ng/mL HGF, or 1 ng/mL TGF-β). Four days later, the indicated proteins were assessed by WB. (*F*) Effect of E-cadherin and Snail double knockdown on the expression of mesenchymal and stem cell markers in Hep3B cells. Six days later, the indicated proteins were assessed by WB. (*G*) IHC of the expression pattern of E-cadherin, CD44, and vimentin using a human HCC tissue array that contains 60 HCC samples (E-cadherin–negative, $n = 28$; –positive, $n = 32$). When the number of E-cadherin–positive cells was <25% of the tumor cell population, the sample was defined as E-cadherin–negative. Representative images of two patients are shown (Magnifications: 40×; insets, 400×.). Data are means ± SD; $^*P < 0.05$.

knockdown was sufficient to up-regulate both EMT and stem cell markers in Hep3B cells, whereas additional supplementation of inflammatory cytokines and/or growth factors was necessary for up-regulation of CD44 in HuH7 and Alexander cells (Fig. 5*E*). Therefore, E-cadherin loss in the tumor cells and inflammatory environment might synergistically up-regulate stem cell markers in our mouse models.

E-cadherin interacts with various molecules and controls activation of related signaling pathways. In our study, increased ERK activation was implicated in accelerated tumorigenesis by loss of E-cadherin. It has been shown that E-cadherin can negatively regulate activation of divergent classes of RTKs such as EGFR, insulin-like growth factor 1 receptor, and c-Met by inhibiting receptor mobility (21); all of this can activate ERK signaling. Our analysis using the phospho-RTK array revealed that deletion of E-cadherin in primary hepatocytes increased EGFR phosphorylation without influencing other RTKs, suggesting that EGFR activation might be one explanation for E-cadherin loss-induced ERK phosphorylation in the liver.

The cellular source of liver cancers is a hot topic at present. *Kras/CDH1*$^{\Delta L}$ mice revealed not only an increase of the ductular reaction but also dysplastic change of ductal cells. These findings, along with CCC and mixed-type tumors, suggested that some tumors might originate from primitive duct cells, including bipotential progenitor cells. However, we also found some well-differentiated hepatocellular lesions that were adjacent to the central vein and distant from proliferating duct cells (Fig. S8*B*), suggesting that they may be derived from mature hepatocytes. In *Kras/CDH1*$^{+/+}$ mice, dysplastic foci were randomly found in zones 1, 2, and 3. Thus, we consider that the tumors in *Kras/CDH1*$^{\Delta L}$ mice may originate from both proliferating duct cells, including progenitor cells induced by inflammation and mature hepatocytes transformed by Ras activation. Meanwhile, recent studies suggested that mature hepatocytes also could transform to CCC (30, 31). Therefore, further analyses such as cell-lineage tracing are needed to definitively determine this issue.

In summary, loss of E-cadherin in the liver, especially in BECs, causes impairment of the intrahepatic biliary network and subsequent inflammatory reactions that lead to progenitor cell proliferation and periductal fibrosis. In some cases, these progenitor cells may lead directly to tumor development through oncogenic mutations such as Kras. In mature hepatocytes, loss of E-cadherin leads to ERK activation, EMT induction, and up-regulation of stem cell markers, which eventually results in enhanced carcinogenesis and an invasive phenotype (Fig. S9). Thus, E-cadherin plays critical roles in maintaining homeostasis and suppressing carcinogenesis in the liver.

Materials and Methods

CDH1$^{F/F}$, *Alb-Cre*, Lox-stop-lox Kras^{G12D}, and Rosa26-lox-stop-lox-YFP mice were purchased from The Jackson Laboratory. *K19*^{CreERT} mice were a generous gift from Guoqiang Gu (Vanderbilt University, Nashville, TN) (18). All mice were on the C57BL/6 genetic background. All animal experiments were approved by the Ethics Committee for Animal Experimentation at the Institute for Adult Diseases, Asahi Life Foundation, University of California, San Diego, and University of Tokyo, and conducted in accordance with the Guidelines for the Care and Use of Laboratory Animals. For details of reagents, biochemical analyses, histology, microarray, cell culture, and statistical analyses, please see *SI Materials and Methods*.

ACKNOWLEDGMENTS. We thank Dr. Alan Hofmann for providing fluorescent-labeled bile acid and Dr. Shoen Kume (Kumamoto University) for handling the mice. This study was supported by a Grant-in-Aid for Scientific Research (25893042 to H.N.; 22300317 and 23114508 to S.M.; 23590933 to Y. Hirata), the Uehara Memorial Foundation (S.M.), and the Daiichi Sankyo Foundation of Life Science (H.N.). Work at the University of California, San Diego, was supported by the National Institutes of Health (CA118165 and CA155120).

1. Gumbiner BM (2005) Regulation of cadherin-mediated adhesion in morphogenesis. *Nat Rev Mol Cell Biol* 6(8):622–634.
2. Stepniak E, Radice GL, Vasioukhin V (2009) Adhesive and signaling functions of cadherins and catenins in vertebrate development. *Cold Spring Harb Perspect Biol* 1(5):a002949.
3. Larue L, Ohsugi M, Hirchenhain J, Kemler R (1994) E-cadherin null mutant embryos fail to form a trophectoderm epithelium. *Proc Natl Acad Sci USA* 91(17):8263–8267.
4. Tunggal JA, et al. (2005) E-cadherin is essential for in vivo epidermal barrier function by regulating tight junctions. *EMBO J* 24(6):1146–1156.
5. Boussadia O, Kutsch S, Hierholzer A, Delmas V, Kemler R (2002) E-cadherin is a survival factor for the lactating mouse mammary gland. *Mech Dev* 115(1-2):53–62.
6. Ihara A, Koizumi H, Hashizume R, Uchikoshi T (1996) Expression of epithelial cadherin and alpha- and beta-catenins in nontumoral livers and hepatocellular carcinomas. *Hepatology* 23(6):1441–1447.
7. Berx G, van Roy F (2009) Involvement of members of the cadherin superfamily in cancer. *Cold Spring Harb Perspect Biol* 1(6):a003129.
8. Matsumura T, Makino R, Mitamura K (2001) Frequent down-regulation of E-cadherin by genetic and epigenetic changes in the malignant progression of hepatocellular carcinomas. *Clin Cancer Res* 7(3):594–599.
9. Lim SO, et al. (2008) Epigenetic changes induced by reactive oxygen species in hepatocellular carcinoma: Methylation of the E-cadherin promoter. *Gastroenterology* 135(6):2128–2140, e8.
10. Lee S, Kim WH, Jung HY, Yang MH, Kang GH (2002) Aberrant CpG island methylation of multiple genes in intrahepatic cholangiocarcinoma. *Am J Pathol* 161(3):1015–1022.
11. Wei Y, et al. (2002) Altered expression of E-cadherin in hepatocellular carcinoma: Correlations with genetic alterations, beta-catenin expression, and clinical features. *Hepatology* 36(3):692–701.
12. Yang MH, et al. (2009) Comprehensive analysis of the independent effect of twist and snail in promoting metastasis of hepatocellular carcinoma. *Hepatology* 50(5): 1464–1474.
13. Ma L, et al. (2010) miR-9, a MYC/MYCN-activated microRNA, regulates E-cadherin and cancer metastasis. *Nat Cell Biol* 12(3):247–256.
14. Lee JM, Dedhar S, Kalluri R, Thompson EW (2006) The epithelial-mesenchymal transition: New insights in signaling, development, and disease. *J Cell Biol* 172(7):973–981.
15. Osada T, et al. (1996) E-cadherin is involved in the intrahepatic metastasis of hepatocellular carcinoma. *Hepatology* 24(6):1460–1467.
16. Malato Y, et al. (2011) Fate tracing of mature hepatocytes in mouse liver homeostasis and regeneration. *J Clin Invest* 121(12):4850–4860.
17. Akagi K, et al. (1997) Cre-mediated somatic site-specific recombination in mice. *Nucleic Acids Res* 25(9):1766–1773.
18. Means AL, Xu Y, Zhao A, Ray KC, Gu G (2008) A CK19(CreERT) knockin mouse line allows for conditional DNA recombination in epithelial cells in multiple endodermal organs. *Genesis* 46(6):318–323.
19. Duncan AW, Dorrell C, Grompe M (2009) Stem cells and liver regeneration. *Gastroenterology* 137(2):466–481.
20. Nakagawa H, et al. (2011) Apoptosis signal-regulating kinase 1 inhibits hepatocarcinogenesis by controlling the tumor-suppressing function of stress-activated mitogen-activated protein kinase. *Hepatology* 54(1):185–195.
21. Qian X, Karpova T, Sheppard AM, McNally J, Lowy DR (2004) E-cadherin-mediated adhesion inhibits ligand-dependent activation of diverse receptor tyrosine kinases. *EMBO J* 23(8):1739–1748.
22. Mani SA, et al. (2008) The epithelial-mesenchymal transition generates cells with properties of stem cells. *Cell* 133(4):704–715.
23. Orsulic S, Huber O, Aberle H, Arnold S, Kemler R (1999) E-cadherin binding prevents beta-catenin nuclear localization and beta-catenin/LEF-1-mediated transactivation. *J Cell Sci* 112(Pt 8):1237–1245.
24. Maeda S, Kamata H, Luo JL, Leffert H, Karin M (2005) IKKbeta couples hepatocyte death to cytokine-driven compensatory proliferation that promotes chemical hepatocarcinogenesis. *Cell* 121(7):977–990.
25. Battle MA, et al. (2006) Hepatocyte nuclear factor 4alpha orchestrates expression of cell adhesion proteins during the epithelial transformation of the developing liver. *Proc Natl Acad Sci USA* 103(22):8419–8424.
26. Rygiel KA, et al. (2008) Epithelial-mesenchymal transition contributes to portal tract fibrogenesis during human chronic liver disease. *Lab Invest* 88(2):112–123.
27. Barrett JC, et al.; UK IBD Genetics Consortium; Wellcome Trust Case Control Consortium 2 (2009) Genome-wide association study of ulcerative colitis identifies three new susceptibility loci, including the HNF4A region. *Nat Genet* 41(12):1330–1334.
28. Yang GH, et al. (2008) Osteopontin combined with CD44, a novel prognostic biomarker for patients with hepatocellular carcinoma undergoing curative resection. *Oncologist* 13(11):1155–1165.
29. Guo X, et al. (2012) Expression features of SOX9 associate with tumor progression and poor prognosis of hepatocellular carcinoma. *Diagn Pathol* 7:44.
30. Fan B, et al. (2012) Cholangiocarcinomas can originate from hepatocytes in mice. *J Clin Invest* 122(8):2911–2915.
31. Sekiya S, Suzuki A (2012) Intrahepatic cholangiocarcinoma can arise from Notch-mediated conversion of hepatocytes. *J Clin Invest* 122(11):3914–3918.

Supporting Information

Nakagawa et al. 10.1073/pnas.1322731111

SI Materials and Methods

Reagents. The following antibodies were used in these experiments: anti–E-cadherin, anti–phospho-ERK, anti-vimentin, and anti-CD44 for Western blotting (Cell Signaling); anti-CD44 for immunohistochemistry and anti-CD44v6 (AbD Serotec); anti-Sox9 and anti-K19 (Santa Cruz Biotechnology); anti–N-cadherin (Millipore); anti-actin and anti-tubulin (Sigma); anti-EpCAM (Abcam); anti–α-smooth muscle actin (Dako); anti-CD45 (eBioscience); anti-F4/80 (Caltag); anti-Ki67 (GeneTex); anti–α-fetoprotein (AFP) (Biocare Medical); anti–β-catenin (GeneTex and BD Transduction Laboratories); and anti-Snail (Novus Biologicals). Recombinant human TNF-α, hepatocyte growth factor, and TGF-β were purchased from R&D Systems.

Immunoblotting. Whole-liver protein homogenates were subjected to SDS/PAGE and transferred to a polyvinylidene membrane (Amersham Biosciences). The membrane was probed with primary antibodies and then incubated with the secondary antibody. Immunocomplexes were detected using the ECL System (Amersham Biosciences). Phospho-RTK (receptor tyrosine kinase) array was performed using the Proteome Profiler Mouse Phospho-RTK Array Kit (R&D Systems) according to the manufacturer's protocol.

RNA Extraction and Real-Time PCR. RNA was extracted from liver tissue using ISOGEN (Nippon Gene). First-strand cDNA was synthesized using SuperScript 2 (Invitrogen Life Technologies), and the relative amount of each mRNA was quantified by real-time PCR and normalized against GAPDH mRNA expression. Primer sequences are available upon request.

Histology. Livers were fixed in 10% (vol/vol) neutral-buffered formalin or 4% (wt/vol) paraformaldehyde, embedded in paraffin, sectioned, and stained with hematoxylin and eosin (H&E) or Sirius red, and processed for immunohistochemistry. In the case of immunostaining of E-cadherin, perfusion fixation was performed with 4% paraformaldehyde. For frozen block preparation, liver tissue was embedded in Tissue-Tek OCT compound (Sakura Finetek). For immunohistochemistry, fixed and paraffin-embedded liver sections were deparaffinized and incubated in citrate buffer at 95 °C for 40 min for antigen retrieval, and then incubated overnight at 4 °C with the primary antibodies. Biotinylated secondary antibodies (Pharmingen) were added and incubated for 20 min at room temperature. Streptavidin-horseradish peroxidase (Pharmingen) was added, and after 30 min the sections were developed with 3,3′-diaminobenzidine substrate and counterstained with hematoxylin. Quantification of the stained area was performed with ImageJ software (National Institutes of Health). Frozen slides were incubated with primary antibodies, followed by secondary antibodies labeled with Alexa 488 or 594 (Molecular Probes).

The expression of E-cadherin in human primary sclerosing cholangitis (PSC) samples was analyzed using liver explants and biopsy samples containing medium or large bile ducts. Adjacent nontumor tissue of metastatic liver cancer was used as a normal control. Liver explants were obtained through the Cooperative Human Tissue Network, and biopsy samples for the diagnosis of PSC were obtained at the University of Tokyo with approval of the medical ethics committee of the University of Tokyo and with informed consent.

The tissue array was purchased from US Biomax and contained 60 paired human hepatocellular carcinoma (HCC) and nontumor tissues. When the number of E-cadherin–positive cells was <25% of the tumor cell population, the sample was defined as E-cadherin–negative. CD44 and vimentin expression in the tumors were scored semiquantitatively based on a scale staining pattern of 0–3 (0, all tumor cells are negative; 1, ≤25%; 2, 25–50%; 3, >50% of the tumor cell population is positive for CD44 or vimentin).

TUNEL staining was performed using an ApoAlert DNA Fragmentation Assay Kit (Clontech).

Electron Microscopy. Livers were fixed with 2% glutaraldehyde/0.1 M phosphate buffer (pH 7.4) and then postfixed with 1% osmium tetroxide/0.1 M phosphate buffer (pH 7.4). Fixed samples were embedded in epoxy resin. Ultrathin sections were counterstained with uranyl acetate and observed with a JEOL 1200 EXII electron microscope.

Immunofluorescence Microscopy for Fluorescent-Labeled Bile Acid. Fluorescent-labeled bile acid was kindly provided by Alan Hofmann (University of California, San Diego), and 100 μL of a 2 mM solution was injected into the tail veins of 2-mo-old $CDH1^{F/F}$ and $CDH1^{\Delta L}$ mice. Fifteen minutes after injection, the mice were killed and the removed livers were embedded in OCT compound. Sections from frozen tissues were visualized by fluorescence microscopy.

Adenovirus- and Tamoxifen-Induced Gene Recombination in Vivo. Recombinant adenovirus expressing Cre-recombinase and control empty adenovirus vector were diluted in PBS and i.v. injected into mice (1×10^9 plaque-forming units per mouse). Tamoxifen (TAM) was dissolved in corn oil and intraperitoneally injected (4 mg TAM per mouse).

Microarray Analysis. Microarray analysis was performed using SurePrint G3 Mouse Gene Expression 8 × 60K arrays (Agilent Technologies) according to the manufacturer's protocol. Data were preprocessed using Agilent GeneSpring GX11.

Diethylnitrosamine-Induced Hepatocellular Carcinoma. Diethylnitrosamine (DEN) (Sigma) was dissolved in PBS and injected intraperitoneally into mice (25 mg/kg) on postnatal day 14. Mice were killed after 8 mo, and their livers were removed and examined for visible tumors.

Cell Culture, Transfections, and RNA Interference. HuH7, Alexander, HLF, HepG2, and SK-Hep1 cell lines as well as a human normal hepatocyte cell line were cultured in Dulbecco's modified Eagle medium with 10% FBS. Hep3B cells were cultured in minimum essential medium (MEM) with 2 mM L-glutamine, 0.15% sodium bicarbonate, 0.1 mM nonessential amino acid solution, 1 mM sodium pyruvate, and 10% FBS. JHH4 cells were cultured in MEMa with 10% FBS. Li7 cells were cultured in RPMI-1640 with 10% FBS. Mouse primary hepatocytes were isolated by the collagenase perfusion method and then cultured in William's E medium with 10% FBS on collagen-coated plates.

A small interfering RNA (siRNA) construct was obtained with siGENOME SMARTpool reagents (Dharmacon), and siRNA transfections were performed using RNAiMAX (Invitrogen). pCMV3 myc-tagged RasG12V plasmid was transfected into normal human hepatocyte cell lines using X-tremeGENE HP DNA Transfection Reagent (Roche). Subcellular protein fractionation was performed using the ProteoExtract Subcellular Proteome Extraction Kit (Calbiochem).

Invasion Assay. An invasion assay was performed using a BD BioCoat Matrigel invasion chamber containing 8.0-μm pore size polyethylene terephthalate membrane inserts in a 24-well format, according to the manufacturer's protocol. Briefly, 5 d after transfection with E-cadherin or control siRNA, 1×10^4 cells were added to the upper chambers in serum-free culture media. The lower chamber

contained 10% FBS. After 24 h, cells on the upper surface of each membrane were removed with cotton swabs, and those that successfully migrated to the lower surface were stained with the Diff-Quick Kit (Sysmex, Japan) and counted. Data are expressed as the percent invasion through the Matrigel and membrane relative to the number of cells migrating through the control membrane.

Mice. $APC^{F/F}$ mice have been described previously (1).

Statistical Analyses. Statistical analyses were performed using the Student *t* test or one-way analysis of variance followed by the Tukey–Kramer test for multiple comparisons. A *P* value <0.05 indicated statistical significance.

1. Grivennikov SI, et al. (2012) Adenoma-linked barrier defects and microbial products drive IL-23/IL-17-mediated tumour growth. *Nature* 491(7423):254–258.

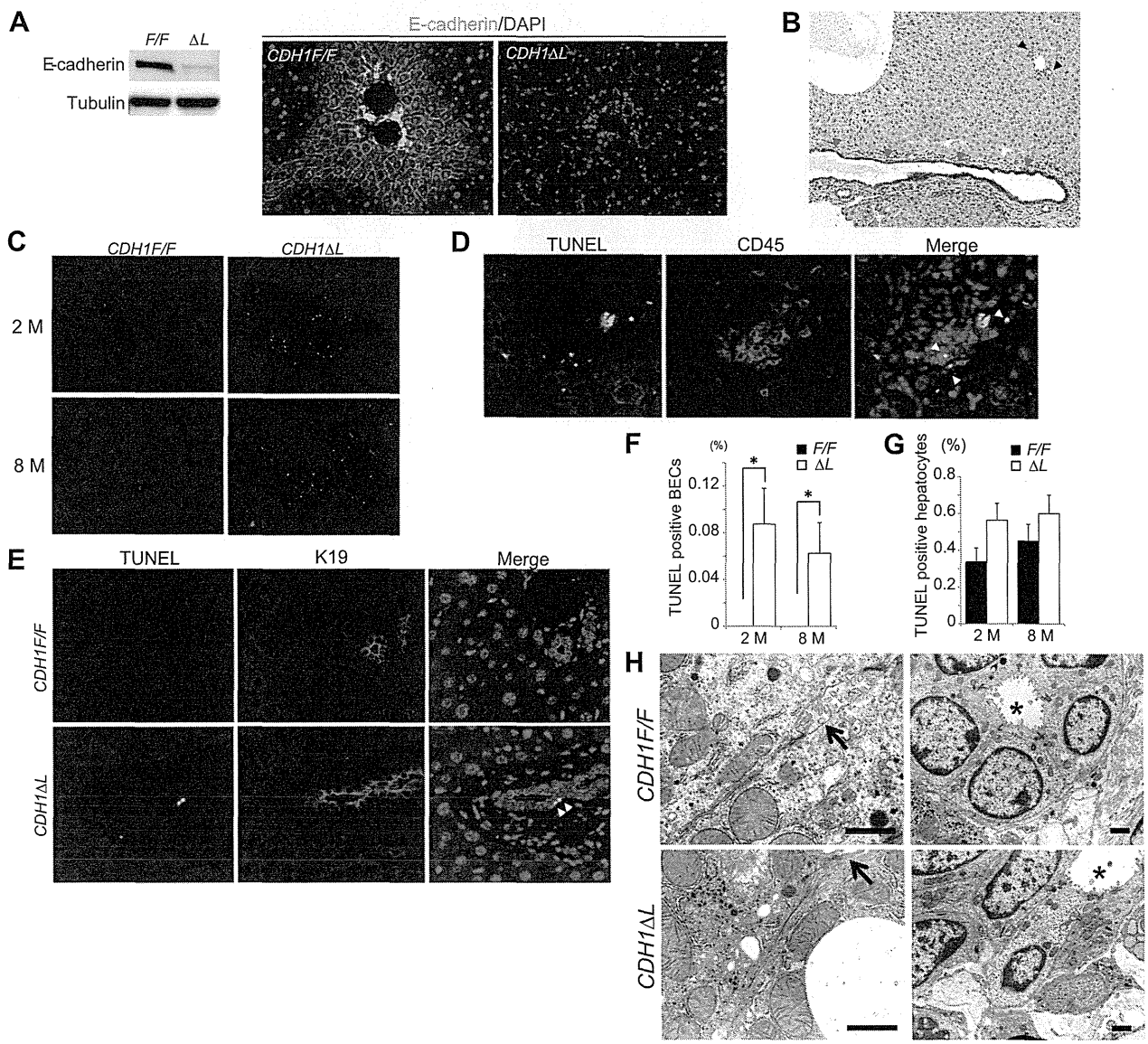

Fig. S1. Characterization of $CDH1^{\Delta L}$ mouse livers. (*A*) Analysis of E-cadherin expression by Western blotting of total liver protein and immunofluorescence (IF) staining of liver sections obtained from 1-mo-old $CDH1^{F/F}$ and $CDH1^{\Delta L}$ mice (×200). Nuclei were labeled with DAPI (blue). (*B*) Immunohistochemistry (IHC) analysis of E-cadherin expression in 1-mo-old $CDH1^{\Delta L}$ mouse liver. Expression of E-cadherin was absent in the interlobular bile duct (black arrowheads) but not in the large bile duct near the common bile duct (red arrowheads) (×200). (*C*) Representative TUNEL-stained sections in 2- and 8-mo-old $CDH1^{F/F}$ and $CDH1^{\Delta L}$ mouse livers (×200). (*D*) Double IF staining of TUNEL (green) and pan-leukocyte marker CD45 (red) in the periportal area of 2-mo-old $CDH1^{\Delta L}$ mouse liver (×400). Arrowheads indicate TUNEL-CD45 double-positive cells. (*E*) Double IF staining of TUNEL (green) and biliary epithelial cell (BEC) marker K19 (red) in 2-mo-old $CDH1^{F/F}$ and $CDH1^{\Delta L}$ mouse livers (×400). Arrowheads indicate TUNEL-K19 double-positive cells. (*F* and *G*) Frequencies of TUNEL-positive duct cells (*F*) and hepatocytes (*G*) in 2- and 8-mo-old $CDH1^{F/F}$ and $CDH1^{\Delta L}$ mouse livers. Data are expressed as means ± SEM ($n = 8$ per group; $^*P < 0.05$.). (*H*) Electron microscopic images of junction complexes in hepatocytes (*Left*) and bile duct cells (*Right*) in 2-mo-old $CDH1^{F/F}$ and $CDH1^{\Delta L}$ mice. (Scale bars, 1 μm.) Arrows and asterisks indicate bile canaliculi and bile duct lumens, respectively.

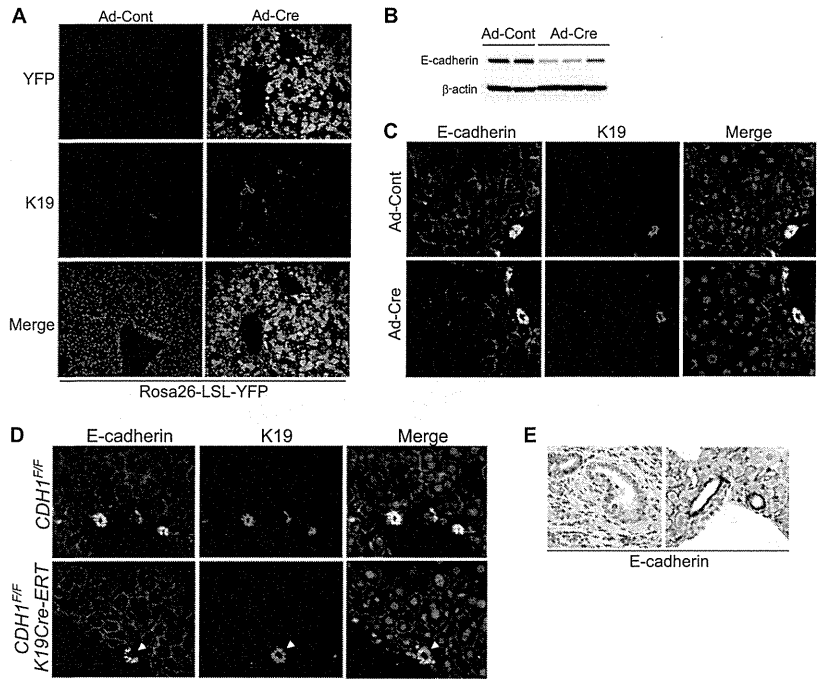

Fig. S2. Separated analysis of the role of E-cadherin in hepatocytes and BECs to maintain liver homeostasis. (*A*) Ad-Cre or Ad-Cont (control adenovirus) was i.v. injected into Rosa26-lox-stop-lox-YFP mice, and 1 wk later, hepatocyte-specific Cre-loxP recombination was confirmed by double IF staining of YFP (green) and K19 (red) (×200). (*B* and *C*) Analysis of E-cadherin expression in *CDH1*$^{F/F}$ mouse liver at 8 wk after Ad-Cre or Ad-Cont injection. Western blotting of total liver protein shows significant reduction of E-cadherin protein in Ad-Cre–injected mice compared with Ad-Cont–injected mice (*B*). Double IF staining of E-cadherin (green) and K19 (red) shows that expression of E-cadherin in hepatocytes was frequently deleted, whereas that in BECs was well-preserved (×400) (*C*). (*D*) TAM was intraperitoneally injected into *CDH1*$^{F/F}$ and *CDH1*$^{F/F}$*K19*^{CreERT} mice, and 1 wk later, BEC-specific deletion of E-cadherin was confirmed by double IF staining of E-cadherin (green) and K19 (red) (×400). Arrowheads indicate E-cadherin–deleted K19-positive BECs. (*E*) IHC analysis of E-cadherin expression in *CDH1*$^{F/F}$/*K19*^{CreERT} mouse liver at 8 wk after TAM injection (×400). (*Left*) Efficient deletion of E-cadherin in BECs with strong periductal inflammation. (*Right*) Inefficient deletion without inflammation. Arrowheads indicate efficiently E-cadherin–deleted bile duct.

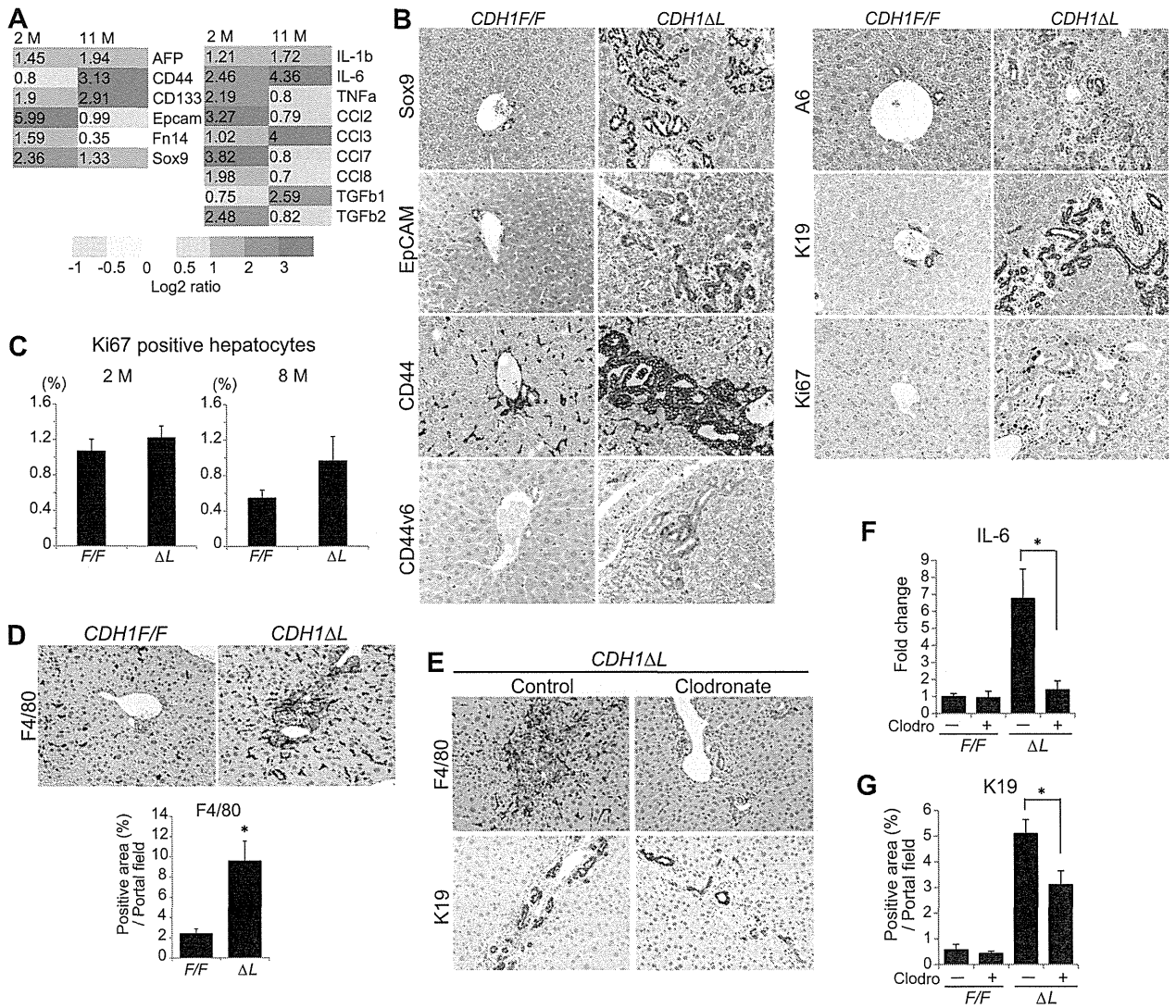

Fig. S3. Ductular reaction in *CDH1*$^{\Delta L}$ mice. (*A*) cDNA microarray analysis of whole-liver samples from *CDH1*$^{F/F}$ and *CDH1*$^{\Delta L}$ mice at 2 and 11 mo of age. Expression of stem cell markers (*Left*) and inflammatory cytokines and chemokines (*Right*) is up-regulated in *CDH1*$^{\Delta L}$ mice compared with *CDH1*$^{F/F}$ mice. Representative genes are shown and data are expressed as log2 ratio. (*B*) IHC analysis of the indicated stem cell and proliferation markers in 8-mo-old *CDH1*$^{F/F}$ and *CDH1*$^{\Delta L}$ mice (×400). (*C*) Frequencies of Ki67-positive hepatocytes in 2- and 8-mo-old *CDH1*$^{F/F}$ and *CDH1*$^{\Delta L}$ mouse livers. Data are expressed as means ± SEM (n = 4–6 per group). (*D*) IHC analysis of F4/80 in 8-mo-old *CDH1*$^{F/F}$ and *CDH1*$^{\Delta L}$ mice (×200). The bar graph shows F4/80-positive areas. Data are expressed as means ± SD (n = 5 per group; *$P < 0.05$). (*E–G*) Effect of macrophage depletion on the ductular reaction. Two-month-old *CDH1*$^{F/F}$ and *CDH1*$^{\Delta L}$ mice were i.v. injected with 100 μL liposomal clodronate or PBS liposome (control) four times every 4 d (days 1, 5, 9, and 13) (n = 3–4 per group). The mice were killed 4 d after the final injection. IHC analysis of the indicated proteins in liposomal clodronate or control-injected *CDH1*$^{\Delta L}$ mice (×200) (*E*). The relative level of IL-6 mRNA was determined by real-time PCR (*F*). K19-positive areas were quantified (*G*). Data are expressed as means ± SD; *$P < 0.05$.

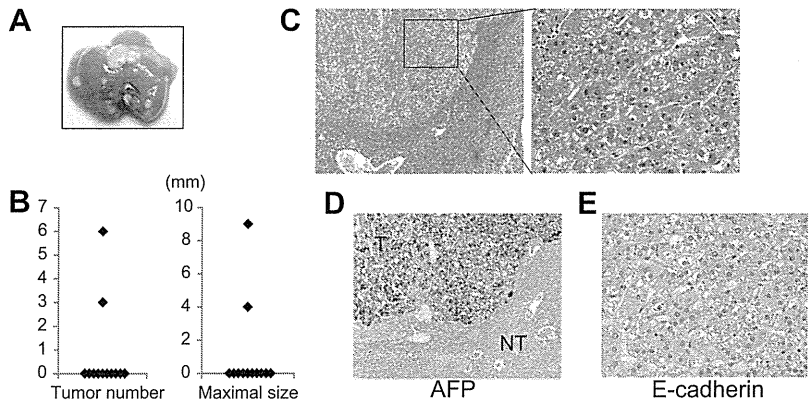

Fig. S4. Some *CDH1*$^{\Delta L}$ mice spontaneously develop liver tumors. (*A*) Representative image of a tumor-bearing liver in an 11-mo-old *CDH1*$^{\Delta L}$ mouse. (*B*) Graphs show tumor number and maximal tumor size in 11-mo-old *CDH1*$^{\Delta L}$ mice ($n = 12$). (*C*) H&E staining of a liver tumor in a *CDH1*$^{\Delta L}$ mouse (*Left*, ×100; *Right*, ×400). (*D* and *E*) IHC analysis of AFP and E-cadherin expression in tumor tissue (*D*, ×100; *E*, ×400). NT, nontumor; T, tumor.

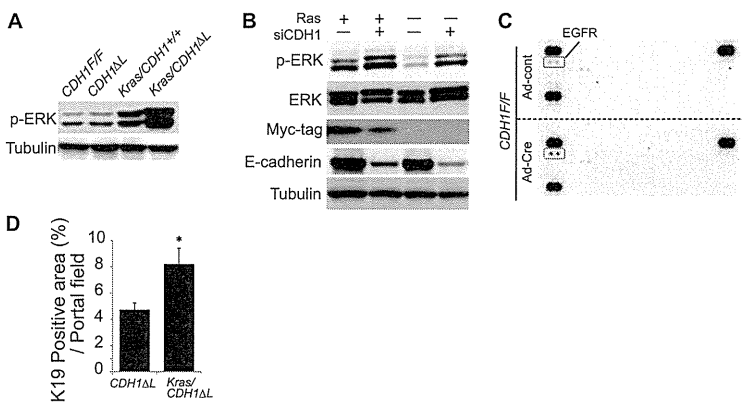

Fig. S5. Cooperative activation of ERK by active Ras and loss of E-cadherin. (*A*) Western blot evaluation of ERK phosphorylation in nontumor tissues of 8-mo-old mouse livers. (*B*) Normal immortalized human hepatocytes were transfected with myc-tagged active Ras (G12V) and siRNA targeted to E-cadherin. The indicated proteins were assessed by Western blotting. (*C*) Primary hepatocytes isolated from *CDH1*$^{F/F}$ mice were infected with Ad-Cont or Ad-Cre and, 48 h afterward, RTK phosphorylation was assessed by phospho-RTK array. (*D*) Quantification of a K19-positive area in 8-mo-old *CDH1*$^{\Delta L}$ and *Kras/CDH1*$^{\Delta L}$ mouse livers (related to Fig. 3*G*). The bar graph shows K19-positive areas. Data are expressed as means ± SD ($n = 5$ per group; $^*P < 0.05$).

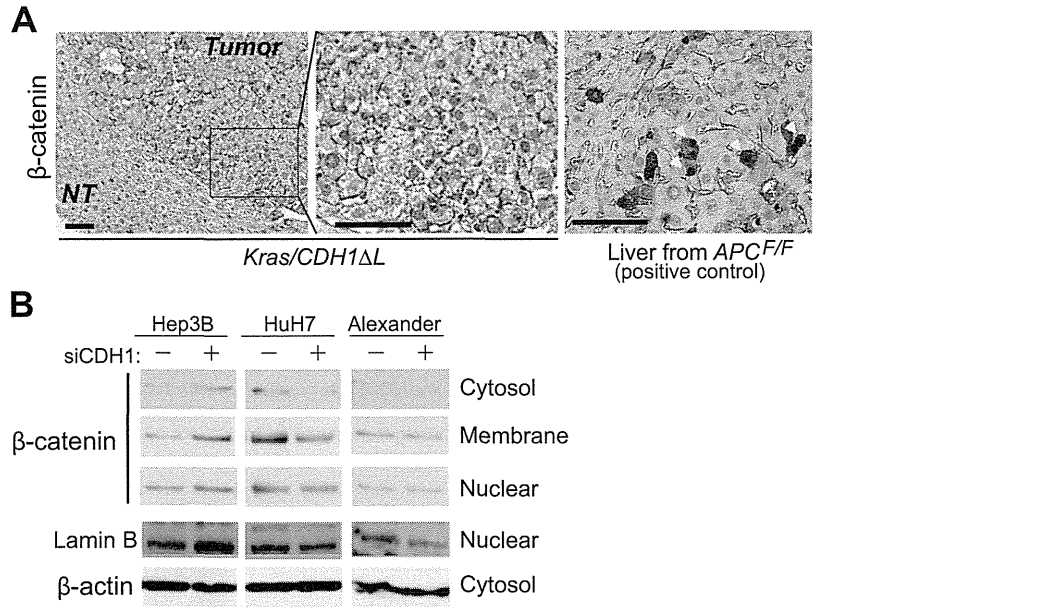

Fig. S6. Effect of E-cadherin loss on β-catenin activation. (*A*) Immunohistochemical analysis of β-catenin expression in tumor and nontumor areas of *Kras/CDH1*$^{\Delta L}$ mouse liver (*Left* and *Center*). (Scale bars, 50 μm.) Liver obtained from an APC flox/flox (*APC*$^{F/F}$) mouse, in which β-catenin/TCF signaling is activated due to reduced APC protein, was used as a positive control (*Right*). Arrowheads indicate hepatocytes positive for nuclear β-catenin. (*B*) Analysis of β-catenin expression in fractionated Hep3B, HuH7, and Alexander cells 6 d after transfection with E-cadherin siRNA or control siRNA. Proteins from the cytosolic, membrane, and nuclear fractions were separated, and β-catenin expression levels were assessed by Western blotting.

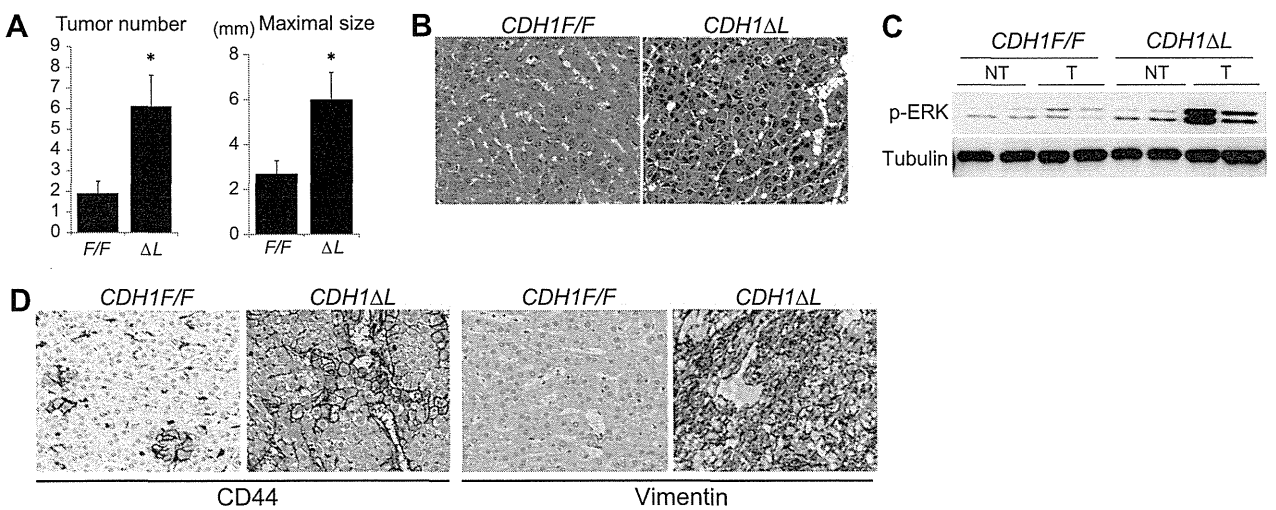

Fig. S7. Loss of E-cadherin promotes DEN-induced HCC. (*A*) *CDH1*$^{F/F}$ ($n = 11$) and *CDH1*$^{\Delta L}$ ($n = 16$) mice were injected with 25 mg/kg DEN on postnatal day 14. After 8 mo, tumor number and tumor size were determined. Data are expressed as the means ± SEM, $^{*}P < 0.05$, compared with *CDH1*$^{F/F}$ mice. (*B*) Representative H&E staining of tumors from DEN-treated *CDH1*$^{F/F}$ and *CDH1*$^{\Delta L}$ mice (×400). (*C*) Western blotting of ERK phosphorylation in NT and T tissues from *CDH1*$^{F/F}$ and *CDH1*$^{\Delta L}$ mice. (*D*) Expression of CD44 and vimentin in tumor tissues from *CDH1*$^{F/F}$ and *CDH1*$^{\Delta L}$ mice was assessed by IHC (×400).

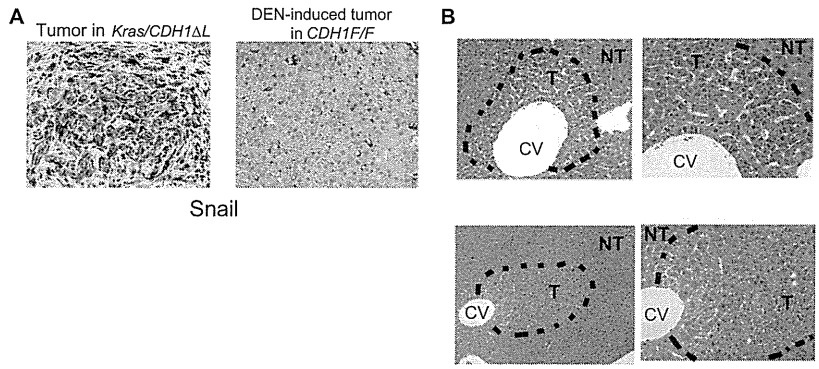

Fig. S8. Characteristics of *Kras/CDH1*$^{\Delta L}$ tumors. (*A*) IHC analysis of Snail in *Kras/CDH1*$^{\Delta L}$ tumors (*Left*, ×400). Tumor cells undergoing epithelial–mesenchymal transition (EMT) strongly expressed Snail. A DEN-induced tumor in *CDH1*$^{F/F}$ mice was used as a negative control (*Right*, ×400). (*B*) Some tumors in *Kras/CDH1*$^{\Delta L}$ mice arise from zone 3. H&E staining images of two representative tumors arising from zone 3 in *Kras/CDH1*$^{\Delta L}$ mice (*Left*, ×200; *Right*, ×400). These tumors are adjacent to the central vein (CV) , which is distant from the portal area.

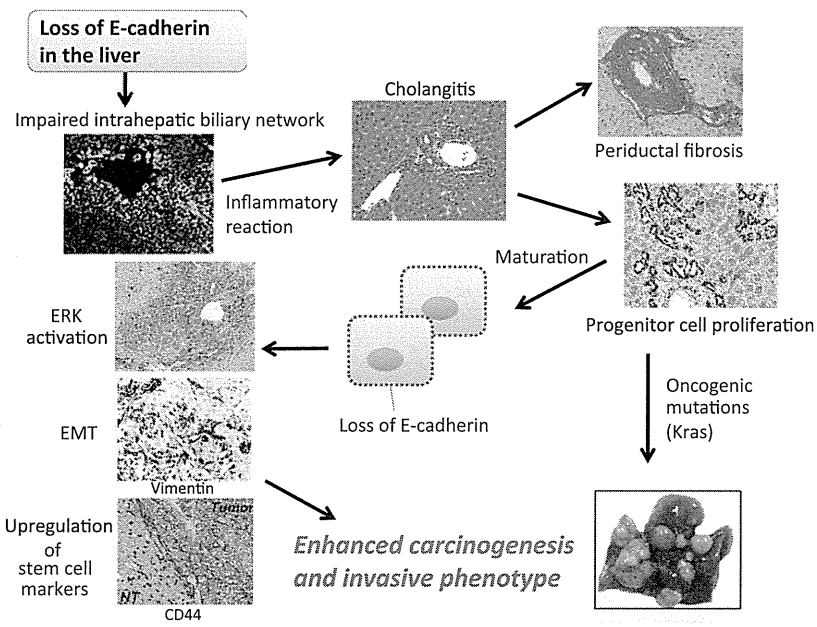

Fig. S9. Proposed mechanism by which loss of E-cadherin induces sclerosing cholangitis and promotes carcinogenesis. Loss of E-cadherin in the liver, especially in BECs, causes impairment of the intrahepatic biliary network and subsequent inflammatory reactions that lead to progenitor cell proliferation and periductal fibrosis. In some cases, these progenitor cells may develop directly into tumors through oncogenic mutations. In mature hepatocytes, loss of E-cadherin leads to ERK activation, EMT induction, and up-regulation of stem cell markers, which eventually results in enhanced carcinogenesis and an invasive phenotype.